

Hybrid Catalysts Comprised of Graphene Modified with Rhodium-Based N-Heterocyclic Carbenes for Alkyne Hydrosilylation

Beatriz Sánchez-Page,^a M. Victoria Jiménez^a Jesús J. Pérez-Torrente,^a Vincenzo Passarelli,^{a,d} Javier Blasco,^b Gloria Subias,^b Marcos Granda^c and Patricia Álvarez*^c*

^a Departamento de Química Inorgánica, Instituto de Síntesis Química y Catálisis Homogénea-ISQCH, Universidad de Zaragoza-C.S.I.C., 50009-Zaragoza, Spain. ^b Instituto de Ciencia de Materiales de Aragón-ICMA, Departamento de Física de la Materia Condensada, CSIC-Universidad de Zaragoza, 50009 Zaragoza, Spain. ^c Instituto Nacional del Carbón, CSIC, P.O. Box, 73, 33080-Oviedo, Spain. ^d Centro Universitario de la Defensa, Ctra. Huesca s/n, ES-50090 Zaragoza, Spain.

CORRESPONDING AUTHOR'S EMAIL:

vjimenez@unizar.es, par@incar.csic.es

ABSTRACT

Thermally partially reduced graphene oxide has been covalently modified with 3-methyl-4-phenyl-1,2,3-triazolium salts making use of the epoxy functionalities on the carbon nanomaterial. Characterization of the functionalized materials through adequate solid characterization techniques, particularly X-ray photoelectron spectroscopy (XPS), allows to follow the stepwise building up of the triazolium fragments on the graphene oxide attached to the wall via covalent C-N linkage. The hydroxyl-triazolium-functionalized materials have been used to prepare rhodium hybrid materials containing either alkoxo or triazolylidene molecular rhodium(I) complexes depending on the protection of the hydroxyl groups present in the material. Characterization of the heterogeneous systems, specially by means of XPS and extended X-ray absorption fine structure (EXAFS) spectroscopy, has evidenced the coordination sphere of the supported rhodium(I) complexes in both rhodium hybrid materials. The graphene-oxide-supported rhodium-triazolylidene hybrid catalysts show excellent activity, comparable to that of the homogeneous [RhI(cod)(Triaz)] (Triaz = 1,4-diphenyl-3-methyl-1,2,3-triazol-5-ylidene) catalyst, for the hydrosilylation of terminal and internal alkynes. In addition, these catalysts have shown good selectivity to the β -(*Z*) vinylsilane isomers (for the not hindered terminal substrates) or *syn*-additions (for the internal substrates). In contrast to the rhodium(I)-alkoxo-based hybrid material, the silyl-protected rhodium(I)-triazolylidene-based hybrid catalyst can be reused in consecutive cycles without loss of activity maintaining the selectivity. The lack of leaching of active rhodium species demonstrate the strength of the C-N covalent bond of the triazolylidene linker to the graphitic wall.

KEYWORDS: graphene, covalent functionalization, hydrosilylation, N-heterocyclic carbenes, rhodium.

INTRODUCTION

Graphene materials have shown promise for heterogeneous catalysis due to their unique electronic behavior, highly aromatic lattice, high surface area or outstanding chemical stabilities, in both alkaline and acid conditions.^{1,2} These properties make them attractive for designing improved hybrid catalytic systems, including covalent grafting, and non-covalent immobilized molecular catalysts.³ In addition, atomically dispersed metal catalysts on graphene materials are also well documented.^{4,5}

To find a simple method to covalently attach the metal complex to the graphene material is the key success factor for designing highly efficient hybrid catalysts. Most of these methods make use of specific oxygen functional groups present on the graphene layer. In this regard, the preparation of graphene by chemical methods produces initially graphene oxide (GO).⁶ The structure of this material exhibits variable amounts of carboxylic acids at the edges/holes and alcohol and epoxy groups (among 10-30 %) at the basal planes of the sheet, disrupting the Csp^2 structure of each sheet and conferring them hydrophilicity and limiting the mass transfer resistance.⁷ Acid groups have been widely used to support organometallic catalysts thus creating ester or an amide bonds.^{8,9} Hydroxyl groups, as on silica surfaces, have also been used to immobilize catalysts mainly via silylation.^{10,11} In contrast, epoxy groups situated at basal planes, although highly abundant in graphene oxide layers have been much less exploited to support the catalysts.^{12,13} The epoxy groups in thermally reduced GO (TRGO) materials, in which the Csp^2 structure is partially reconstructed¹⁴ and the acid groups are selectively eliminated,¹⁵ should allow the development of alternative synthetic routes to effectively immobilize organometallic catalysts minimizing the negative effect of undesired lateral reactions due to acid groups.¹⁶

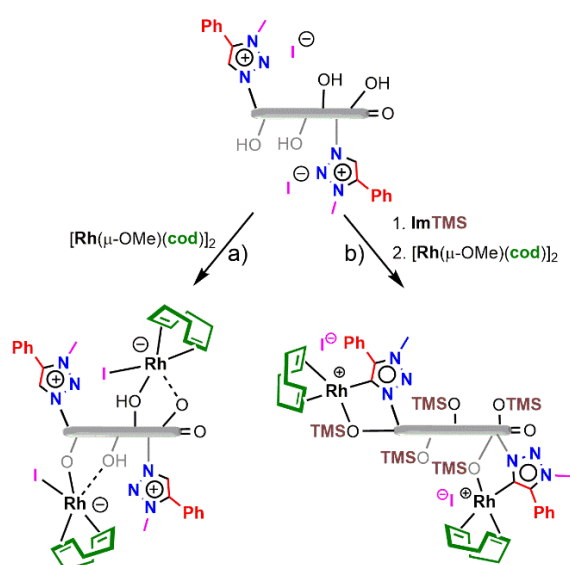
Hydrofunctionalization of unsaturated compounds, the addition of a covalent H-Z bond across a carbon-carbon or carbon-heteroatom multiple bond, is an essential and sustainable

process for the preparation of many useful synthetic intermediates.¹⁷ In this context, transition-metal-catalyzed hydrosilylation of terminal alkynes is a straightforward and atom-economical methodology for the preparation of vinylsilanes.¹⁸ The hydrosilylation of terminal alkynes may yield three vinylsilane isomers: α , β -(Z) and β -(E), although the formation of silylalkyne derivatives, resulting from the competitive dehydrogenative silylation process, is occasionally observed for some catalytic systems. Thus, the control of the chemo-, regio- and stereoselectivity of the reaction is a key issue in transition metal hydrosilylation catalysis.¹⁹ Interestingly, Rh(I) complexes having functionalized N-heterocyclic carbene (NHC) ligands have shown to be efficient catalysts for the hydrosilylation of terminal alkynes showing a marked selectivity towards the formation of the less thermodynamically stable β -(Z) vinylsilane isomer.²⁰ We foresee that the development of recyclable hybrid catalysts with well-defined Rh(I)-NHC active sites attached to the carbon surface has the potential to enhance catalytic performance and catalyst stability not only in the hydrosilylation of alkynes but also in related hydrofunctionalization reactions. In this context, it is worth of mention that a rather limited number of heterogenized rhodium hydrosilylation catalysts have been described so far in the literature.^{21,22} To the best of our knowledge, there are only two examples of Rh(I)-NHC catalysts covalently supported on carbonaceous materials recently reported by Messerle and co-workers,²³ one of which was applied exclusively to the hydrosilylation of the internal alkyne diphenylacetylene.²⁴ In addition, pyrene-tagged rhodium NHC complexes non-covalently immobilized onto reduced graphene oxide have found to be moderately active catalyst for the hydrosilylation of terminal alkynes also with a very limited recyclability.²⁵

We have recently reported the covalent linkage of Ir(I)-NHC complexes to functionalized CNTs and graphene oxide materials via ester or acetyl and carbonate linkers, respectively, to prepare robust active and recyclable catalysts in hydrogen transfer and water oxidation

reactions.^{26,27,28} Unfortunately, these type covalent linkages are unsuitable for the design of GO-based Rh(I)-NHC hybrid catalysts as they are reactive sites under hydrosilylation conditions which could yield leaching of the catalysts.¹⁶ Thus, our approach for the design of robust hybrid hydrosilylation catalysts is to make use of the epoxy groups on the solid surface of a thermally reduced graphene oxide (TRGO) obtained at 400 °C. This new synthetic strategy has allowed the direct construction of triazolylidene covalent linkers on the graphene oxide material following a stepwise solid phase synthesis of the corresponding triazolium fragments. Extended X-ray absorption fine structure (EXAFS) spectroscopy, which is sensitive to the short range order around the photoabsorbing atom,^{26,29} have revealed that the successful preparation of hybrid materials comprising triazolylidene rhodium complexes anchored to the carbon nanomaterial requires protection of the hydroxyl groups still present in the material (Scheme 1).

We report herein on the synthesis and full characterization of these new GO-based Rh(I)-NHC hybrid materials and their application as hydrosilylation catalysts for a range of terminal and internal alkynes with diverse hydrosilanes. In addition, recyclability studies including XPS and HRTEM analysis of the hybrid materials after catalysis are also reported.



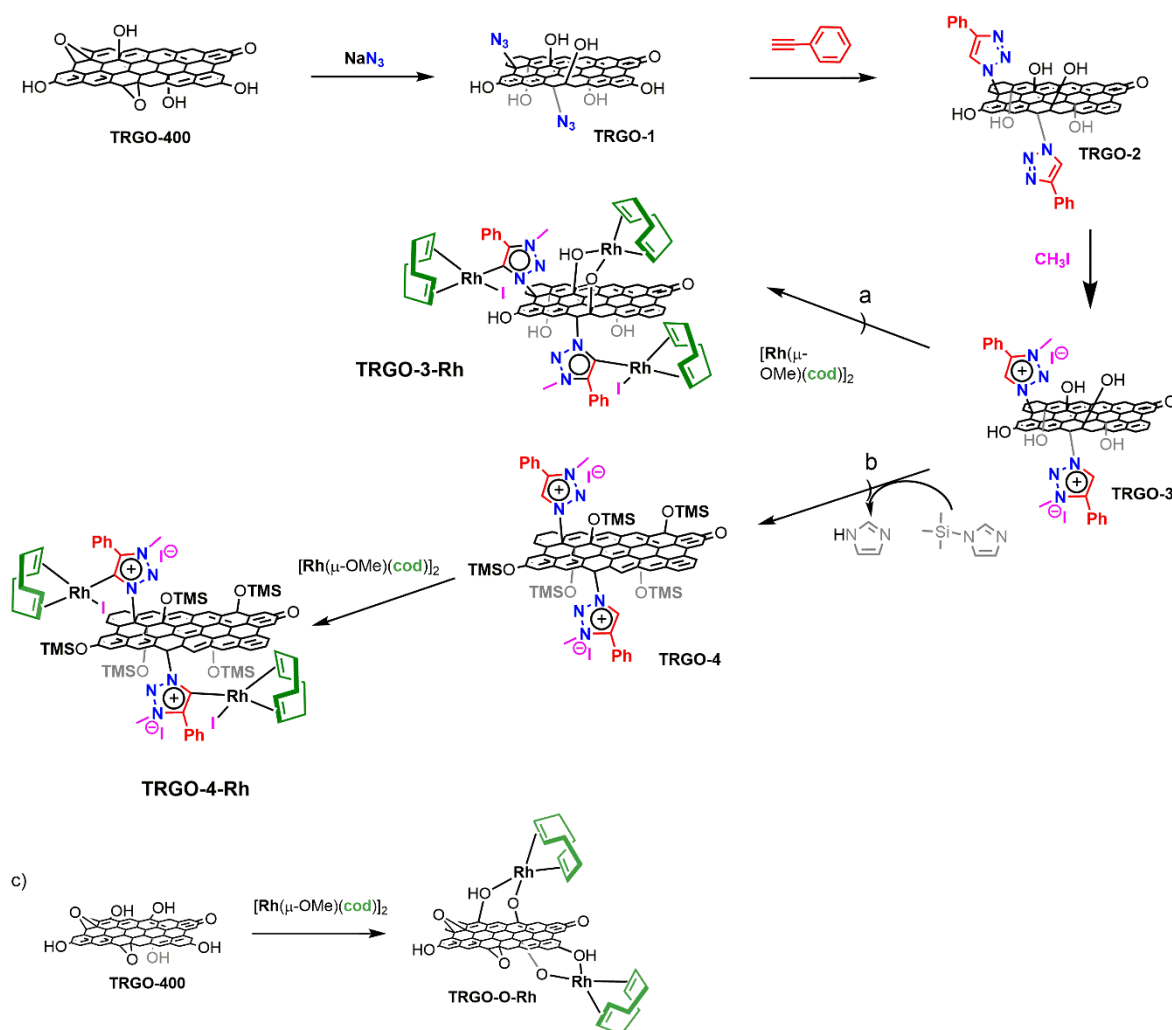
Scheme 1. Schematic synthesis, structure and chemical composition for the new hybrid catalysts.

RESULTS AND DISCUSSION

Synthesis and characterization of triazole-based graphene-NHC materials. A partially reduced graphene oxide, **TRGO-400**, was used in this work to support the Rh-NHC catalysts through triazolylidene covalent linkers. This graphene material was obtained from a graphene oxide by thermal treatment at 400°C. **TRGO-400** is almost free of acid groups but still exhibits certain amount of keto, hydroxyl and epoxy groups at the basal planes, as observed in the XPS C1s analysis (Table S1, Supporting Information) and FTIR⁷ (Figure S6, Supporting Information).

The supporting of the rhodium complex to **TRGO-400** requires the initial generation of the triazolium functionalized graphene sheet. The procedure developed to achieve this covalent linkage follows the three step route outlined in Scheme 2. The first step comprises the 1,2 epoxide ring opening reaction with sodium azide to yield **TRGO-1**.³⁰ As a result, the nitrogen content in this azide-functionalized graphene material increases up to 2.9 wt.%, as determined by elemental analysis (Table S1, Supporting Information). Additionally, the FTIR spectra of **TRGO-1** exhibit, when compared to that of **TRGO-400**, the appearance of the typical azide band at 2121 cm⁻¹ together with an enhancement of the C-OH band at 3200-3600 cm⁻¹ and a decrease of the C-O-C band at 1254 cm⁻¹ (Figure S6, Supporting Information). All these results are consistent with the introduction of the N₃ moiety in the graphene sheets.^{31,32} The atomic nitrogen content in this sample, calculated by XPS analysis, is however lower than expected (0.9 %, Table S1, Supporting Information). Moreover, the broad XPS N1s curve (Figure 1a, yellow curve), despite accounting for a low amount of nitrogen which increases uncertainty, could be consistent with a partial decomposition of the labile azide moiety by action of the XPS irradiation beam.³³ The outcome is an increase of the C-N bonds at <399 eV (corresponding to decomposition products) with respect to that of the characteristic azide =N⁺= component at ~402.8 eV that can still be distinguished.³⁴ In

any case, the XPS C1s spectrum (Table S1, Supporting Information) reveals a slight increment in intensity and broadening of the C-X band, now accounting for C-O and C-N bonds. Additionally, although the C/O ratio is maintained after functionalization, there is a slight change in the distribution of the oxygen functional groups at the graphene basal planes after reaction with azide (Figure 1b, yellow curve) which is ascribed to their different environment before and after functionalization.



Scheme 2. Synthesis and proposed structure of triazole-based graphene-NHC rhodium hybrid catalysts: a) unprotected $-\text{OH}$ groups, b) silyl protected $-\text{OH}$ groups, and c) hybrid Rh(I) material lacking the triazolium pendant groups.

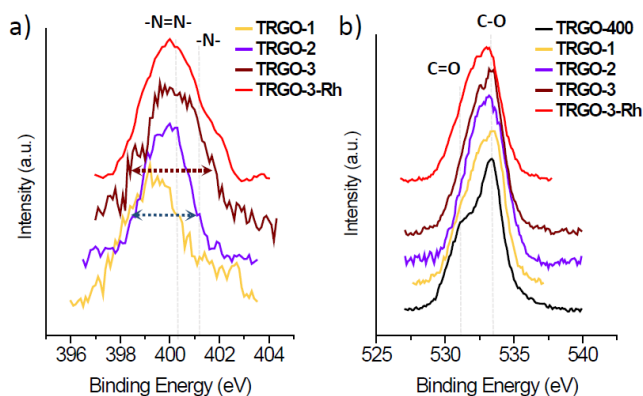


Figure 1. XPS spectra of parent and/or functionalized partially reduced graphene oxides (**TRGO-x**): a) N1s, and b) O1s regions.

By treating **TRGO-1** with phenylacetylene in a mixture of water and 2-propanol (1:1) in the presence of sodium ascorbate (NaAsc) and CuSO_4 as catalyst, the 1,2,3-triazole-decorated material **TRGO-2** was obtained through a Huisgen cycloaddition reaction (click reaction). As a confirmation a clear change in the high-resolution XPS N1s spectra of both materials is observed. Thus, the profile of **TRGO-2** (Figure 1a, purple curve) is narrower than that of **TRGO-1** (Figure 1a, yellow curve) and can be adjusted to the two expected components of the 1,2,3-triazole moiety, that is, -N=N- at ~ 400.0 eV and -N- at ~ 401.1 eV. The average area ratio of both components is 1:2 which correspond to the expected azide cycloaddition structure (see Supporting Information).³⁴ On the other hand, the formation of the N-heterocyclic structure seems to exert little effect on the carbonaceous graphene skeleton since: i) alike deconvolution values of the XPS C1s spectra before and after reaction (Table S1, Supporting Information), ii) similar Raman spectra (see Supporting Information), and iii) similar XPS O1s spectra profiles (Figure 1b, yellow and purple curves), are observed.

Treatment of **TRGO-2** with methyl iodide provokes the quaternization of the nitrogen-3 in the heterocycles providing the required 3-methyl-4-phenyl-1,2,3-triazolium iodide functionalized material, **TRGO-3**. Interestingly, this step broadens the N1s spectra profiles

thus increasing the full width at half maximum (FWHM) of the whole **TRGO-2** (Figure 1a, purple curve) curve from ~1.8 eV to ~2.4 eV in **TRGO-3** (Figure 1a, garnet curve). By means of TGA, the amount of ligand introduced in the graphene sheet, corresponding to the weight loss between 144 and 310 °C, was quantified as 5.8 wt.% (see Supporting Information). Remarkably, the graphene basal planes in **TRGO-3** sheets still exhibit certain amount of free -OH groups, as indicated by the strong and broad absorption peak at ~3400 cm^{-1} in the FTIR spectrum (Figure S6, Supporting Information).

Synthesis and characterization of triazole-based graphene-NHC rhodium hybrid catalysts. *Direct metalation of TRGO-3.* Following the general procedure to prepare NHC-metal complexes from the corresponding azolium salts,³⁵ the triazolium-functionalized material **TRGO-3** was reacted with $[\text{Rh}(\mu\text{-OMe})(\text{cod})]_2$ (cod = 1,5-cyclooctadiene) to give the material **TRGO-3-Rh**. In principle, deprotonation of the weak acid protons of the anchored triazolium groups by the basic methoxo ligands in the dinuclear complex $[\text{Rh}(\mu\text{-OMe})(\text{cod})]_2$ (cod = 1,5-cyclooctadiene) to give 1,2,3-triazol-5-ylidene linkers should be expected. However, it should be noted that due to its acidity the hydroxyl groups on the graphene sheets could compete with the triazolium groups for the coordination of the rhodium center (Scheme 2, a).

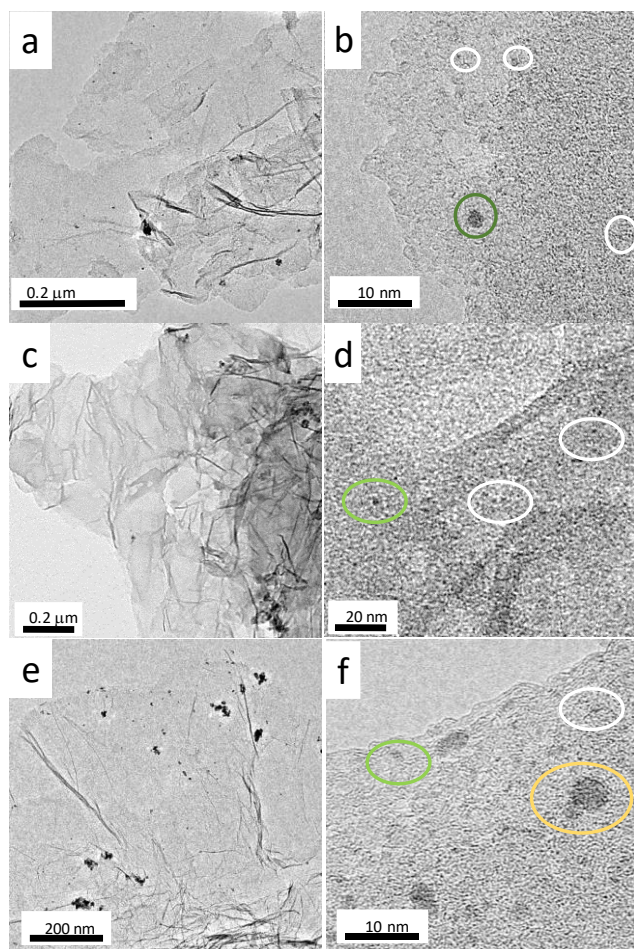


Figure 2. HRTEM images of supported Rh(I) complexes: a) and b) **TRGO-3-Rh**, c and d) **TRGO-4-Rh**, e) and f) **TRGO-O-Rh**.

The amount of Rh in the supported material **TRGO-3-Rh**, determined by means of ICP-MS measurements, is 2.6 wt.%. Taken into account the nitrogen content in this sample (1.3 wt.% by means of elemental analysis, Table S1, Supporting Information) a theoretical functionalization degree of *ca.* 82 % can be estimated by considering only the maximum amount of rhodium that can be loaded on the basis of the nitrogen content (3/1 for a N/Rh atomic ratio). The high-resolution Rh3d XPS spectrum (Figure S18, Supporting Information) of **TRGO-3-Rh** shows, in the region between 306 and 318 eV, the typical doublet with an average separation between maxima of 4.6 eV as well as a maximum of the 3d5/2 peak (range of ~306–311 eV) centered at ~308.7 eV. All of this is in agreement with

the formation of Rh(I) organometallic complexes.^{36,37} The HR-TEM images of **TRGO-3-Rh** (Figure 2a,b) and the quantitative energy dispersive X-ray spectroscopy (EDX) mapping (see Supporting Information) confirm the homogeneous distribution of this supported Rh(I)-NHC complexes (small size electrodense regions, 0.2–0.6 nm, black spots representative marked with white circles) all throughout the graphenic basal planes. Medium size rhodium particles are also detected (up to 2 nm, Figure 2 b, green circle) in a relatively high amount in the HR-TEM images. These might be clusters³⁸ or nanoparticles³⁹ possibly formed during beam irradiation,^{¡Error! Marcador no definido.¡Error! Marcador no definido.} though they could also be related to the wider structural heterogeneity of the supported complexes in **TRGO-3-Rh** due to competitive metalation along the supporting process, as stated before. In this regard, an analysis of the XPS N1s and O1s spectra of **TRGO-3-Rh** evidences some peculiarities in this sample. On one hand, the XPS N1s spectra of **TRGO-3-Rh** (Figure 1a, red curve) exhibit a profile quite similar to that of **TRGO-3**. This likeness suggests the presence of non-deprotonated triazolium groups in the graphene material since not significant changes in binding energies were observed after Rh support. Moreover, the support of the Rh(I) fragment strongly modifies the profile of the XPS O1s spectra (Figure 1b). Thus, an increase of the intensity in the signal at lower binding energies is observed in **TRGO-3-Rh** (~531 eV, Figure 1c, red curve), with respect to that of **TRGO-3** (Figure 1b, garnet curve). This effect accompanies also an increment of the C-X bond in the C1s spectra (Table S1, Supporting Information) for the **TRGO-3-Rh** material. These facts could be in line with the implication of hydroxyl functional groups in the supporting reaction. Therefore, the expected Rh(I)-triazolydine supported complexes might be also accompanied by another Rh(I) complexes linked to deprotonated hydroxyl groups on the wall of **TRGO-3** (Scheme 2, a). Thus, there could be two very different molecular rhodium(I) complexes anchored in **TRGO-3**, one with coordination sphere formed by a diene, an iodido, and a 1,2,3-triazol-5-

ylidene, and the second one formed by a diene, an alkoxo, and a hydroxyl both on the carbon material wall.

In order to gain more insights into the local structure of Rh(I) atoms, EXAFS spectra at the Rh K-edge were measured for both the hybrid material, **TRGO-3-Rh**, and the related molecular complex **[RhI(cod)(Triaz)]** (Triaz = 1,4-diphenyl-3-methyl-1,2,3-triazol-5-ylidene) (Scheme S1). Rh foil and Rh₂O₃ were also measured as references. As expected, the energy edge positions of Rh(I) catalysts (~23.224 keV) are at intermediate values of the two references (see Figure S27, Supporting Information). The Fourier transform (FT) of the weighted EXAFS signal, $k^2\chi(k)$, of **TRGO-3-Rh** is shown in Figure 3a. The first peak of the FT modulus at $R \sim 1.67 \text{ \AA}$ (without phase shift correction) agrees with Rh-C bond lengths while the second strong peak at $R \sim 2.35 \text{ \AA}$ corresponds to the longer Rh-I distance. The occurrence of an iodine atom in the first coordination shell of Rh atom seems to point to the direct bond of Rh to the triazolylidene group together with iodido and cod ligands. As the resulting local structure around Rh atoms is very similar to that of complex **[RhI(cod)(Triaz)]** (see below), we tried to fit the EXAFS spectrum of **TRGO-3-Rh** using the structural data of **[RhI(cod)(Triaz)]**. Although the fit seemed to be reasonable, some refined distances were at odds. In particular, an interatomic Rh-N distance between Rh and triazolylidene group was extremely short (below Rh-I distance) whereas other Rh-C from the same ring were exceedingly high and located beyond the fit range. These facts strongly disagree with a Rh-triazolylidene structure for **TRGO-3-Rh** as initially thought (Scheme 2, a) and consequently, the anchoring of the Rh(cod) fragment to the graphene surface through triazolylidene linkers is discarded. In addition, the comparison of both EXAFS spectra **TRGO-3-Rh** and **[RhI(cod)(Triaz)]** showed additional significant differences (see Supporting Information and later EXAFS results on this manuscript).

The next step was considering the anchoring of the Rh(cod) fragment through the hydroxyl groups followed by the replacing of one oxygen by an iodine atom. The fit was also reasonable but a visual inspection of the plot clearly showed the lack of another contribution to a smaller distance from the Rh-I path as can be inferred from the partial overlap of the two peaks in the FT modulus (Figure 3a and Supporting Information). In the first model, this partial overlap was solved by the above mentioned short Rh-N path. As Rh-N and Rh-O paths have similar scattering amplitudes (similar Z), we hypothesized that an iodido ligand has been added to the coordination sphere of the metal in addition to the proposed structure for the rhodium complex in red trace. Accordingly, the new Rh-O path, slightly shorter than Rh-I path, solved partial overlapping between the two peaks in the FT curves yielding a good fit to the experimental data as can be seen in the Figure 3a.

Based on this analysis, a new structure for **TRGO-3-Rh** is proposed (Figure 3b). The triazolium salt has not been deprotonated and remains anchored to TRGO as in the precursor material **TRGO-3**, whereas the RhI(cod) fragment binds to a deprotonated hydroxyl group coming from the graphitic support thereby resulting in an anionic metal complex. In addition, another surface-hydroxyl group remains coordinated at longer distances via an attractive Van der Waals force. In general lines, this result also agrees with the lack of significant changes in the XPS N1s spectrum (Figure 1a, red curve).

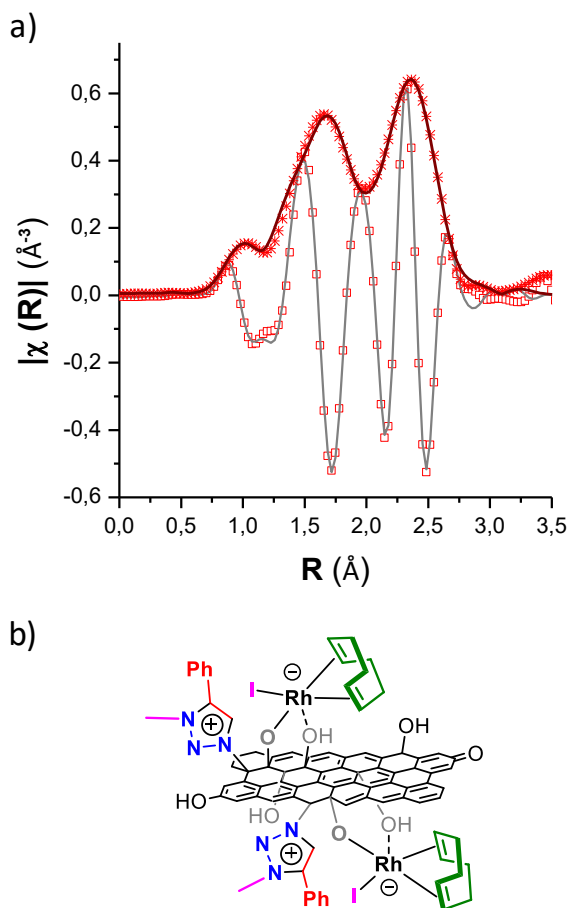


Figure 3. a) Best fits (lines) and experimental (points) FTs curves (asterisks for the modulus and squares for the real part) of the k^2 -weighted EXAFS signal, extracted between 2.9 and 15 \AA^{-1} using a sinus window, for **TRGO-3-Rh**. b) Structure of **TRGO-3-Rh** in accordance with the EXAFS analysis. Refined distances (\AA): Rh-O = 2.037(14), Rh-C (x4) = 2.164(14), Rh-I = 2.649(9) and Rh-O = 2.514 (27). Rest of refined parameters can be found in Supporting Information.

Silyl protection of the -OH groups in TRGO-3 and metalation. With the **TRGO-3-Rh** structure deduced from the EXAFS analysis in hand and in order to avoid the interference of hydroxyl groups, the protection of all -OH groups in **TRGO-3** (those coming from the reaction of the epoxide with the azide and those originally existing in the starting material **TRGO-400**) was performed prior to the reaction with the dinuclear rhodium-methoxo precursor by reaction of **TRGO-3** with trimethylsilylimidazole⁴⁰ (Scheme 2, b). The

successful silyl protection of the hydroxyl groups is observed in the XPS spectra of the **TRGO-4**, giving a Si atomic content of 5.3 % (Table S1, Supporting Information). Moreover, the C-O bonds of the C-O-Si(CH₃)₃ moiety are clearly identified in the XPS O1s as a signal of appreciable intensity at high binding energies (533.7 eV, Figure 4a, dark-green curve). In addition, the FTIR spectra also show the typical C-O-Si functional groups at ~1100 cm⁻¹ (Figure S6, Supporting Information).

Treatment of the silyl-protected material **TRGO-4** with the dinuclear complex [Rh(μ -OMe)(cod)]₂ produces the deprotonation of the weak acid H5 proton of the triazolium groups yielding **TRGO-4-Rh** where all the rhodium environments are supposed to be formed by the cyclooctadiene, the 1,2,3-triazol-5-ylidene, and an iodido as ligands (Scheme 2, b). A 5.2 wt.% of Rh was determined for **TRGO-4-Rh** by means of ICP-MS measurements, while the nitrogen content is 2.7 wt.% (elemental analysis, Table S1, Supporting Information). These data allow to estimate a 79 % of functionalization for this sample assuming a N/Rh atomic ratio of 3/1 in the supported triazolium complex.

For comparative purposes, we have also prepared a hybrid Rh(I) material lacking the triazolium pendant groups, **TRGO-O-Rh** (blank material), by reacting **TRGO-400** directly with the Rh(I) precursor [Rh(μ -OMe)(cod)]₂. In this later case, the coordination sphere of all the metal centres should be composed by the alkoxo group, the diene, and likely another nearby hydroxyl group of the wall (Scheme 2, c). The amount of Rh in **TRGO-O-Rh**, determined by means of ICP-MS analysis, increases up to 7.7 wt.%. This comparatively high value makes sense based on the large number of linking sites in the graphene sheet, hydroxyl functional groups in this case, higher than the amount of triazolium pendant groups in **TRGO-4** or even in **TRGO-3**.

The high resolution XPS Rh 3d spectrum of **TRGO-4-Rh** exhibits the typical doublet with an average separation between maxima of 4.6 eV⁴¹ with the maximum of the 3d_{5/2} peak at

ca. 308.7 eV (Figure 4b, green curve). In contrast the blank material **TRGO-O-Rh** (Figure 4b, blue-dashed curve) exhibits a shoulder at lower eV (307.5 eV) which could correspond to a partial portion of Rh(0) species. These rhodium nanoparticles could be probably formed in the absence of the triazolium pendant group after the addition of the precursor $[\text{Rh}(\mu\text{-OMe})(\text{cod})]_2$ due to the reducing character of the graphene material.

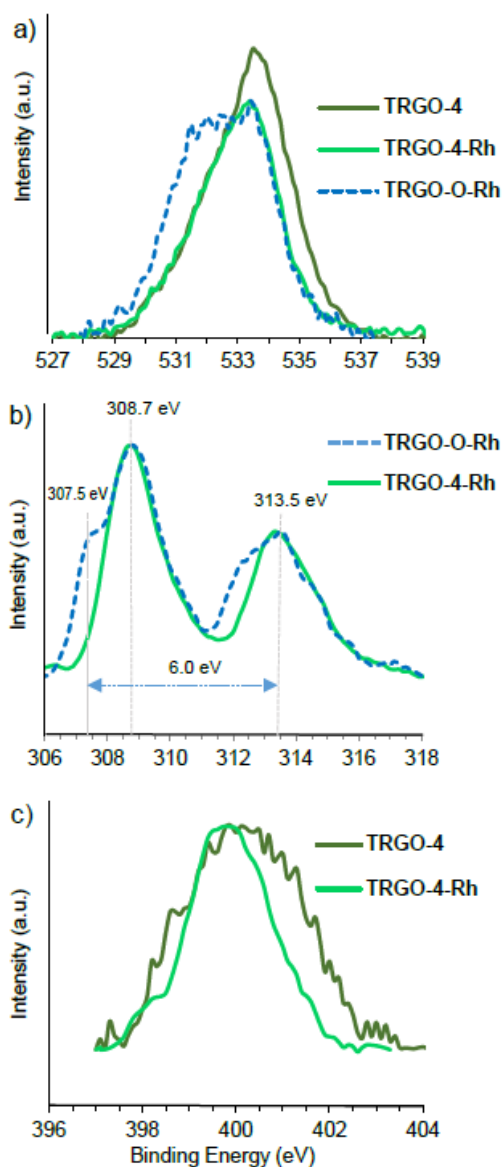


Figure 4. XPS spectra of **TRGO-4** and Rh-supported hybrid materials **TRGO-4-Rh** and **TRGO-O-Rh**: a) O1s, b) Rh3d, and c) N1s regions.

The XPS N1s band of **TRGO-4-Rh** (Figure 4c, green curve) confirms the presence of the triazolium moiety (similar profile than **TRGO-4**, dark-green curve). Additionally, this signal becomes narrower after supporting the metal center (FWHM varying from ~ 2.5 eV in **TRGO-4** to ~ 1.9 eV in **TRGO-4-Rh**) what suggests the coordination of the triazolylidene fragment to rhodium. It is important to note that this feature was not observed in the XPS N1s profile of **TRGO-3-Rh**. Moreover, in contrast to what was also observed for **TRGO-3-Rh** (Figure 1b, red curve), the anchoring process marginally modified the O1s XPS curve profile (Figure 4a, dark-green and green curves). In addition, a slight shift of the C-O-Si band towards lower binding energies was observed for **TRGO-4-Rh** compared to the parent material that could be ascribed to some kind of interaction with the rhodium center in the former (see EXAFS analysis below).

HRTEM images (Figure 2c, 2d) and STEM-EDX mapping (see Supporting Information) of **TRGO-4-Rh** shows a homogeneous distribution of supported rhodium complexes with electron-dense regions of small size (black spots of 0.2–0.6 nm, Figure 2c, white circles) throughout the graphenic basal planes. Interestingly, medium size particles (up to 2 nm, Figure 2c, green circles), which were relatively abundant in **TRGO-3-Rh**, decrease in number in **TRGO-4-Rh** probably as a result of a greater structural homogeneity of this later sample. As expected, silicon also appears uniformly distributed all over the graphenic plane (see STEM-EDX mapping, Supporting Information). On the other hand, HRTEM images of **TRGO-O-Rh** shows the presence of much larger electron-dense regions (up to 6 nm, Figure 2e, 2f, brown circles) together with small/medium size electron-dense regions (white-green circles), making the distribution of rhodium in this sample less homogeneous. This heterogeneous distribution in this sample could be also in agreement with the formation of clusters of rhodium nanoparticles or clusters and rhodium single organometallic compounds as a result of the absence of the triazolium pendant group in the parent material.

EXAFS spectrum of **TRGO-4-Rh** was collected under the same conditions used to measure that of **TRGO-3-Rh**. The absorption edge position also agrees with a Rh(I) complex (Figure S27, Supporting Information). Figure 5a shows the FT (real part and modulus) of the $k^2\chi(k)$ signal extracted between 2.9 and 15 \AA^{-1} using a sinus window. The first peak of the FT modulus at $R\sim 1.62 \text{ \AA}$ (without phase shift correction) agrees with Rh-C bond lengths and it is more intense than the one observed previously for **TRGO-3-Rh** (compare Figure 3a and Figure 5a). However, the second peak located at $R\sim 2.54 \text{ \AA}$ is significantly smaller for **TRGO-4-Rh** and hard to reconcile with the presence of iodide in the first coordination shell of rhodium atoms. These facts resemble the properties of related iridium-hybrid catalysts where a halogen atom is replaced by an oxygen from an $-\text{OH}$ functional group of the TRGO surface.²⁶ Therefore the model to analyze the EXAFS spectra was based on the structure of $[\text{RhI}(\text{cod})(\text{Triaz})]$ but replacing the Rh-I path with a Rh-O one. The fit is also plotted in the Figure 5a and the reliability factor is $R_F = 0.005$. Accordingly, the structure of **TRGO-4-Rh** is in agreement with the plot of Figure 5b and details of the refined parameters can be found in the Supporting Information.

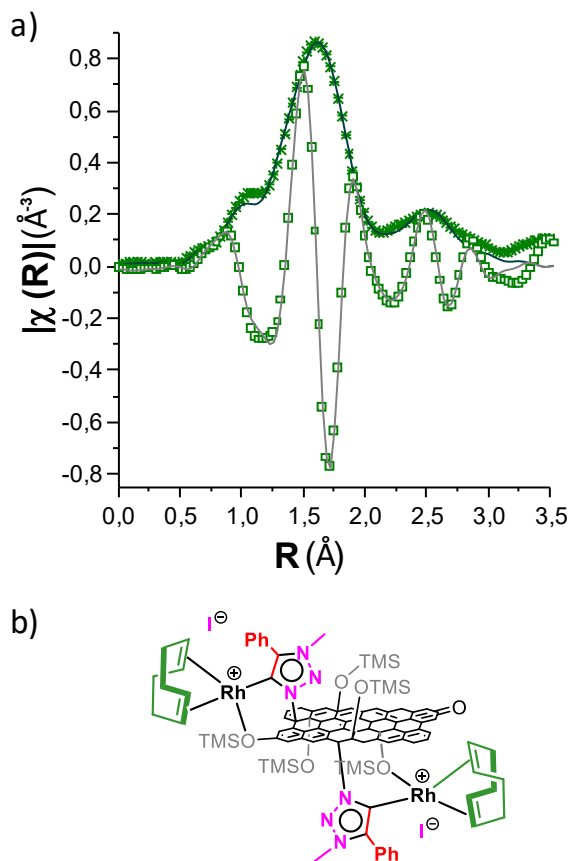


Figure 5. a) Best fits (lines) and experimental (points) FTs curves (asterisks for modulus and squares for the real part) of the k^2 -weighted EXAFS signal for **TRGO-4-Rh**. b) Structure of **TRGO-4-Rh** in accordance with its EXAFS analysis. Refined distances (\AA): Rh-O = 2.032(3), Rh-C = 2.032(3) and Rh-C (x4) = 2.151(14). Rest of refined parameters can be found in the Supporting Information.

Synthesis and Characterization of the molecular catalyst [RhI(cod)(Triaz)] related to the hybrid catalysts TRGO-4-Rh. With the aim to compare the activity/structure of related hybrid and homogeneous catalysts, we have prepared the molecular complex **[RhI(cod)(Triaz)]** (Triaz = 1,4-diphenyl-3-methyl-1,2,3-triazol-5-ylidene) following the general procedure entailing the reaction of the corresponding triazolium salt with 0.5 equiv of $[\text{Rh}(\mu\text{-OMe})(\text{cod})]_2$ in THF at room temperature. The triazolium salt, 1,4-diphenyl-3-methyl-1,2,3-triazolium iodide, precursor of the triazolylidene ligand, was prepared via the well-known “click reaction” involving a copper-catalyzed [3+2] cycloaddition of

phenylazide and phenylacetylene (Scheme S1, Supporting Information).⁴² The related chlorido compound [RhCl(cod)(Triaz)] was previously prepared by Albretch et al. using a classical transmetalation procedure involving the triazolium iodide salt, Ag₂O and [Rh(μ -Cl)(cod)]₂.⁴³

Complex **[RhI(cod)(Triaz)]** was isolated as a yellow solid in good yield and characterized by elemental analysis, mass spectroscopy and standard spectroscopic techniques. The neutral character of the compound was evidenced by conductivity measurements in acetone. In addition, the high resolution electrospray mass spectrum showed a peak at m/z ratio of 446.118, which corresponds to the molecular ion without the iodido ligand. The ¹H NMR spectrum confirms the deprotonation of the triazolium fragment, and in consequence, the expected coordination of the NHC ligand to the rhodium center what becomes evident in the ¹³C{¹H} NMR spectrum with the characteristic upfield doublet resonance for the carbenic carbon atom of the 1,2,3-triazol-ylidene ring at δ 174.7 ppm ($J_{\text{Rh-C}} = 44.5$ Hz). These chemical shifts lie in the usual range for related Rh^I-NHC complexes.^{44,45} In accordance with the proposed structure, the ¹H NMR spectra showed two resonances for the =CH olefinic protons of the cod ligand but four doublet resonances ($J_{\text{Rh-C}} = 7\text{-}14$ Hz) were seen in the ¹³C{¹H} NMR spectra which is in agreement with the lack of an effective symmetry plane in the molecule, probably as a result of the hindered rotation around the carbene-rhodium bond in the unsymmetrical NHC ligand (see Supporting Information).⁴⁶

All this gathered information was in accordance with the crystal structure of **[RhI(cod)(Triaz)]**. The complex exhibits a square planar geometry at the metal centre with a *cis* disposition of the iodido ligand and of the triazole moiety (Figure 6a). The bidentate cod ligand occupies the remaining coordination sites, thus rendering an overall geometry similar to that already observed in the chlorido derivative [RhCl(cod)(Triaz)].⁴⁷ As for the triazole ligand, the C(1)-C(2)-N(3)-N(4)-N(5) ring lays almost perpendicular to the

coordination plane [I–Rh–C(1)–C(2) 101.2(3)°] and adopt an almost ideal arrangement with respect to the Rh–C(1) bond [θ 1.0, ψ 2.3°,⁴⁸ cf. Figure 6a]. Remarkably different dihedral angles are observed between the two phenyl rings and the triazole core [C(17)–C(12)–N(5)–C(1) -24.7(5)°, C(1)–C(2)–C(6)–C(7) -46.0(4)°]. In this connection, two factors should be decisive, namely the steric hindrance of the C(18)-methyl group and the C(17)-H(17)···Rh anagostic interaction, H(17)···Rh, 2.4760(3), C(17)–H(17)–Rh 132.30.^{49,50} Relevant intermolecular contacts in the crystal structure of **[RhI(cod)(Triaz)]·CHCl₃** are described in the Supporting Information.

EXAFS spectrum of **[RhI(cod)(Triaz)]** was also recorded and Figure 6b shows the FT (real part and modulus) of the $k^2\chi(k)$ signal extracted between 2.9 and 15 Å⁻¹ using a sinus window. The FT modulus displays two strong peaks without overlapping in contrast to what was observed in the **TRGO-3-Rh** material (compare Figures 3a and 6b). With the structural data of **[RhI(cod)(Triaz)]** in hand, the fit was very good with a reliability factor of $R_F = 0.09$ and the refined distances are in agreement with the data obtained from X-ray diffraction measurements.

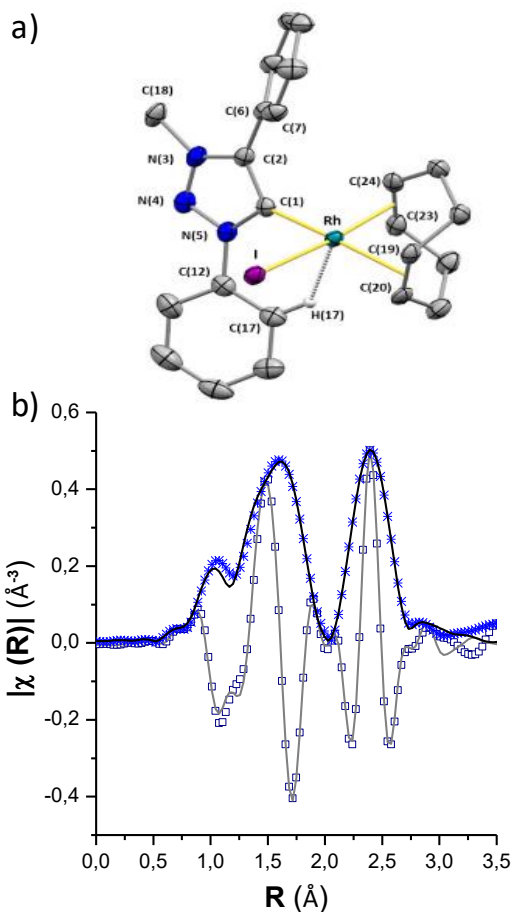


Figure 6. a) ORTEP view of **[RhI(cod)(Triaz)]** with thermal ellipsoids at 50 %. Selected bond lengths (Å) and angles (°) are: Rh–I 2.6771(3), Rh–C(1) 2.036(3), Rh–Ct1 2.1090(3), Rh–Ct 2 2.0032(2), C(1)–Rh–I 89.21(8), Ct1–Rh–Ct2 87.151(9), I–Rh–C(1)–C(2) 101.2(3), C(17)–C(12)–N(5)–C(1) -24.7(5), C(1)–C(2)–C(6)–C(7) -46.0(4). Ct1, centroid of C(19) and C(20); Ct2, centroid of C(23) and C(24). b) Best fits (lines) and experimental (points) FTs curves (asterisks for modulus and squares for the real part) of the k^2 -weighted EXAFS signal for **[RhI(cod)(Triaz)]**. Refined distances (Å): Rh–C(1) = 2.092(7), Rh–C(23) = 2.098(7), Rh–C(24) = 2.098(7), Rh–C(19) = 2.19(7), Rh–C(20) = 2.19(7) and Rh–I = 2.706(6). Rest of refined parameters can be found in the Supporting Information;

Catalytic activity in hydrosilylation of alkynes and recycling of heterogeneous catalysts. The rhodium hybrid catalysts **TRGO-3-Rh** and **TRGO-4-Rh** and the related homogeneous catalyst **[RhI(cod)(Triaz)]** were tested as catalyst precursors for the

hydrosilylation of alkynes under the reaction conditions previously optimized for Rh(I)-catalyzed hydrosilylation of terminal alkynes.²⁰ The catalytic reactions were performed in CDCl₃ or acetone-*d*₆, at 25 or 60 °C, with standard catalyst loads of 1 mol% and routinely monitored by ¹H NMR spectroscopy using anisole as internal standard. A range of aliphatic and aromatic terminal alkynes, including oct-1-yne, phenylacetylene and 3,3-dimethyl-but-1-yne, were efficiently reduced to the corresponding vinylsilane derivatives using HSiMePh₂, HSiMe₂Ph, and HSiEt₃ as hydrosilanes (Table 1). Hydrosilylation of terminal alkynes can result in a complicate mixture of products: (*Z*)- or (*E*)-1-silyl-1-alkenes, products from the anti-Markovnikov addition, and 2-silyl-1-alkene from the Markovnikov addition and dehydrogenative silylation products, alkynylsilane and the corresponding alkene (Scheme S2, Supporting Information).

The hydrosilylation of oct-1-yne with HSiMe₂Ph catalyzed by **[RhI(cod)(Triaz)]** in CDCl₃ does not proceed at room temperature. However, the reaction was almost completed at 60 °C in a little more than half an hour, giving 98 % selectivity to β-(*Z*)-vinylsilane (entries 1 and 2). The reaction with HSiMePh₂ is slower but gives full conversion to the β-(*Z*) isomer in 1 hour (entry 9). The hybrid catalysts **TRGO-3-Rh** and **TRGO-4-Rh** are also efficient catalysts for the hydrosilylation of alkynes giving full conversion in 1-1.5 h. However, a slight decrease in the selectivity for the β-(*Z*)-vinylsilane isomer was observed (entries 3-4 and 10-11), particularly with the silyl-protected hybrid catalyst **TRGO-4-Rh** and the less reactive hydrosilane HSiMePh₂.

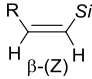
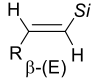
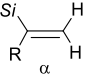
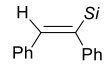
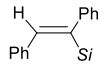
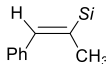
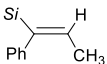
In general, the catalytic systems are slightly more active in acetone-*d*₆ as solvent. In fact, **[RhI(cod)(Triaz)]** and **TRGO-3-Rh** are active at room temperature. The homogeneous catalyst exhibited an excellent catalyst performance, both in terms of activity and selectivity, in the hydrosilylation of oct-1-yne with both hydrosilanes (entries 5 and 12). However, in the case of **TRGO-3-Rh** a significant drop in the selectivity was observed at room

temperature (entry 6). In contrast, **TRGO-4-Rh**, which is inactive at room temperature, showed an excellent performance at 60 °C giving almost full conversion in one hour with selectivity for the β -(Z)-vinylsilane isomer of around 85 % (entries 8 and 13). Interestingly, catalyst **[RhI(cod)(Triaz)]** gave full conversion to the corresponding β -(Z)-vinylsilane isomer in the hydrosilylation of oct-1-yne with the aliphatic hydrosilane, HSiEt₃, both in CDCl₃ at 60 °C and in acetone-*d*₆ at room temperature (entries 14 and 17). Under these conditions, both hybrid catalysts showed good activities although poor selectivity (entries 15-18 and 16-19). It is worth mentioning that the catalyzed isomerization of β -(Z)-vinylsilane to the more thermodynamically stable β -(E)-vinylsilane isomer or to the corresponding allyl-silyl derivatives, frequently observed in the case of linear alkyl chain alkynes once the alkyne substrate has been completely consumed, here is not observed.^{†Error!}

Marcador no definido.^{51,52}

A reverse selectivity toward the β -(E)-vinylsilane isomer of 48 % and 38 % for **[RhI(cod)(Triaz)]** and **TRGO-4-Rh**, respectively, together with significant amounts of alkene (*ca.* 30 %), resulting from the competitive dehydrogenative silylation, were observed in the hydrosilylation of a bulky aliphatic alkyne such as *t*-Bu-C \equiv CH with HSiMe₂Ph (entries 20 and 21) which is in agreement with the observed trend for rhodium(I) catalysts containing alkylamino-functionalized NHC ligands.²⁰ Finally, the hydrosilylation of phenylacetylene with HSiMe₂Ph by the hybrid catalysts **TRGO-3-Rh** and **TRGO-4-Rh** resulted in the massive formation of polyphenylacetylene even at room temperature, in fact a 84 % selectivity for polyphenylacetylene was attained with **TRGO-4-Rh** after 30 min of reaction in CDCl₃ at 60 °C (entry 23).⁵³ Although the polymerization was inhibited in the case of **[RhI(cod)(Triaz)]** in CDCl₃, the catalyst exhibited a moderated catalytic activity and poor selectivity (entry 22).

Table 1. Hydrosilylation of Alkynes by Homogeneous and Hybrid Triazolylidene Rhodium(I) Catalysts.^{a,b}

entry	alkyne/ silane	solvent	T (°C)	Catalyst	t (h)	conv (%)	Selectivity (%) ^c		
									
1	<i>n</i> -HexC≡CH	CDCl ₃	25	[RhI(cod)(Triaz)]	2	5	99	<0.1	<0.1
2	/HSiMe ₂ Ph		60	[RhI(cod)(Triaz)]	0.6	98	99	0.6	0.4
3			60	TRGO-3-Rh	0.8	99	94	5	1
4			60	TRGO-4-Rh	1	95	92	5	3
5		acetone- <i>d</i> ₆	25	[RhI(cod)(Triaz)]	1	98	94	6	-
6			25	TRGO-3-Rh	5	60	56	34	10
7			60	TRGO-3-Rh	1.3	98	76	21	3
8			60	TRGO-4-Rh	0.7	96	82	13	5
9	<i>n</i> -HexC≡CH	CDCl ₃	60	[RhI(cod)(Triaz)]	1	98	99	<0.1	<0.1
10	/HSiMePh ₂		60	TRGO-3-Rh	0.8	99	93	6	1
11			60	TRGO-4-Rh	1.4	99	82	12	6
12		acetone- <i>d</i> ₆	25	[RhI(cod)(Triaz)]	2	98	90	8	2
13			60	TRGO-4-Rh	1	97	86	14	-
14	<i>n</i> -HexC≡CH	CDCl ₃	60	[RhI(cod)(Triaz)]	2.4	98	98	<1	<1
15	/HSiEt ₃		60	TRGO-3-Rh	1.5	97	70	14	16
16			60	TRGO-4-Rh	1.6	98	53	27	20
17		acetone- <i>d</i> ₆	25	[RhI(cod)(Triaz)]	2	95	99	<0.1	<0.1
18			60	TRGO-3-Rh	1	95	60	30	10
19			60	TRGO-4-Rh	3	97	89	5	6
20 ^d	<i>t</i> -BuC≡CH/	acetone- <i>d</i> ₆	25	[RhI(cod)(Triaz)]	3.5	97	25	40	20
21 ^d	HSiMe ₂ Ph		60	TRGO-4-Rh	5	99	24	38	10
22	PhC≡CH/	CDCl ₃	60	[RhI(cod)(Triaz)]	7.5	97	60	26	14
23 ^e	HSiMe ₂ Ph		60	TRGO-4-Rh	0.5	96	16	-	-
									
24	PhC≡CPh/	CDCl ₃	60	[RhI(cod)(Triaz)]	1	99	96	4	
25	HSiMe ₂ Ph		60	TRGO-4-Rh	3	99	99	<0.1	
26		acetone- <i>d</i> ₆	25	[RhI(cod)(Triaz)]	0.6	98	99	<0.1	
27			60	TRGO-4-Rh	1.5	98	99	<0.1	
									
28	PhC≡CMe/	CDCl ₃	60	[RhI(cod)(Triaz)]	1.8	96	46	54	
29	HSiMe ₂ Ph		60	TRGO-4-Rh	1	98	50	50	
30		acetone- <i>d</i> ₆	25	[RhI(cod)(Triaz)]	1.5	98	80	20	
31			60	TRGO-4-Rh	1	99	55	45	

a) Conversions and selectivities (%) were calculated by ¹H NMR using anisole as internal standard. b) Experiments were carried out in CDCl₃ or acetone-*d*₆ (0.5 mL) using a HSiR₃/RC≡CR'/catalyst ratio of 100/100/1, [catalyst]₀ = 2 × 10⁻³ M in homogeneous systems and 1 mol% of Rh in heterogeneous systems calculated according to the ICP measurements. c) Si = SiR₃. d) 15 and 28 % of *t*-BuCH=CH₂ were produced, respectively. e) PPA, polyphenylacetylene, was produced in 84 %.

The reaction profiles of conversion and selectivity versus time for the hydrosilylation of oct-1-yne with HSiMe₂Ph catalyzed by [RhI(cod)(Triaz)] and TRGO-4-Rh, obtained by monitoring the reactions by ¹H NMR. [RhI(cod)(Triaz)] is somewhat more active than TRGO-4-Rh providing a 95 % of conversion in 30 min with a 95 % of selectivity for the β-(Z)-vinylsilane isomer (Figure 7a). TRGO-4-Rh gave an 84 % conversion in 30 min under the same conditions and a 75 % of selectivity for the β-(Z)-vinylsilane isomer (Figure 7b). In general terms, both types of catalysts present very similar reaction profiles that suggest a similar operating mechanism (see Supporting Information).

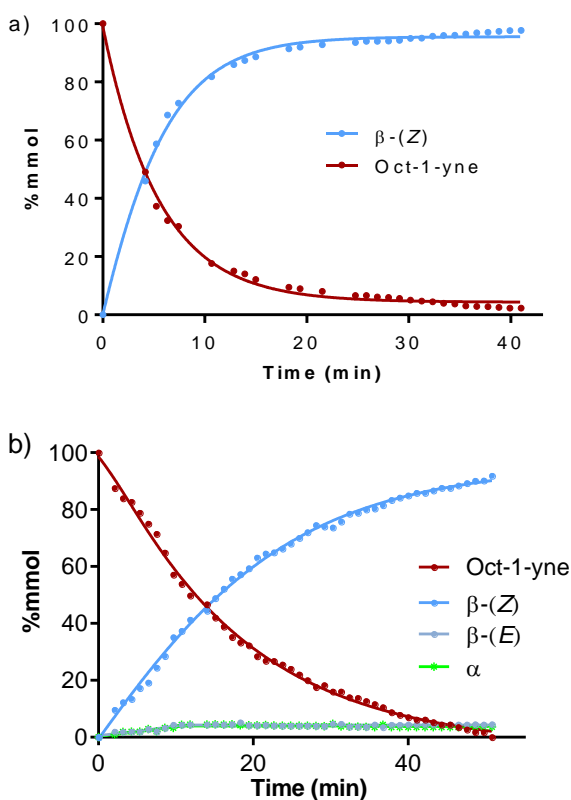


Figure 7. Reaction profile of conversion and selectivity obtained from ¹H NMR data for the hydrosilylation of oct-1-yne with HSiMe₂Ph (1:1) in CDCl₃ (0.5 mL) at 60 °C catalyzed by: a) [RhI(cod)(Triaz)], [catalyst]₀ = 2 x 10⁻³ M, 1 mol%, and b) TRGO-4-Rh, 1 mol% of Rh calculated according to the Rh-ICP measurement.

The homogeneous and hybrid catalysts were also applied for the hydrosilylation of internal alkynes (Table 1). The hydrosilylation of diphenylacetylene with HSiMe₂Ph catalyzed by [RhI(cod)(Triaz)] in CDCl₃ does not proceed at room temperature but it was completed in one hour at 60 °C to afford a 96 % selectivity to the *E*-vinylsilane isomer, the *syn*-addition reaction product (entry 24). The reaction is faster in acetone-*d*₆ at room temperature showing a slight improvement of selectivity (entry 26). The hybrid catalyst **TRGO-4-Rh** showed an excellent catalytic performance affording practically full conversion to the *E*-vinylsilane isomer both in CDCl₃ and in acetone-*d*₆ at 60 °C (entries 25 and 27). The hydrosilylation of 1-phenyl-1-propyne proceeds efficiently in both solvents to afford roughly an equimolar mixture of the two possible *syn*-addition reaction products (entries 28-31).

Catalyst recycling experiments have been carried out with the heterogeneous catalysts **TRGO-3-Rh** and **TRGO-4-Rh** using the hydrosilylation of oct-1-yne with HSiMePh₂ in CDCl₃ at 60 °C as model reaction. For comparative purposes, the catalytic activity of **TRGO-O-Rh**, which is considered as a reaction blank, has been also studied (Table 2). The recycling studies (run *n*) of the heterogeneous catalysts were carried out by evaporating the solvent under vacuum washing the residue with fresh *n*-hexane (3 x 1 mL), and then subjected to another catalytic cycle by addition of further HSiMePh₂/oct-1-yne/CDCl₃. In addition, in order to control possible rhodium leaching along the catalytic runs, the catalytic activity of the CDCl₃ solutions obtained after removing the heterogeneous catalyst has also been studied in some cases by addition of successive loads of reactants.

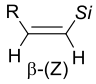
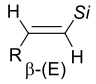
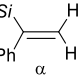
As it was expected, the catalytic activity of the material **TRGO-O-Rh** decreased in the first recycling run (run 2), reaching less than half the conversion in a reaction time three times longer (entries 1 and 2). The catalytic activity of **TRGO-3-Rh** gradually decreased after successive catalytic runs as evidenced by the longer reaction times required to reach conversions higher than 90 % (entries 3-5). Thus, in accordance with the proposed structure

for **TRGO-3-Rh**, the linker of the molecular rhodium catalyst to the carbon graphene oxide is easily broken under catalytic conditions leading to leaching. As a confirmation, the solutions obtained after removing the heterogeneous catalyst exhibited catalytic activity (entries 6-8, loads 2-4). Further, the catalytic activity of the solutions also dropped after successive loads of reactants, which points to progressive catalyst deactivation in solution.

Interestingly, the recycled supported catalyst **TRGO-4-Rh** exhibited the same catalytic performance as the fresh catalyst after 4 consecutive cycles. The recycling runs were performed under an argon atmosphere except the last run that was carried out under air. The catalytic reactions were monitored by NMR showing kinetic profiles in the successive experiments very similar to that plotted in Figure 7b, even for the last cycle. As it can be seen in Table 2, comparable activities and selectivities were observed in similar recycling experiments in the hydrosilylation of oct-1-yne with HSiMe_2Ph (entries 15-19). The hybrid catalyst **TRGO-4-Rh** also showed an excellent recycling performance in the hydrosilylation of oct-1-yne using HSiMePh_2 (entries 9-13) or HSiEt_3 (entries 20-23) as hydrosilanes, and in the hydrosilylation of the internal alkyne 1-phenyl-1-propyne (entries 24-26).

The stability of the immobilized rhodium complex on the surface of **TRGO-4-Rh** was checked by analyzing by ICP/MS spectra of the filtrate and washings after each run in the hydrosilylation of oct-1-yne with HSiMePh_2 (Table 2, entries 9-13) to determine their Rh content. An initial 3% loss of Rh from the material surface was observed after the first cycle (Figure S41, Supporting Information) which is consistent with the initial removal of the physisorbed rhodium species, not eliminated by the standard washing of the material but likely removed under the reaction conditions of the catalysis.

Table 2. Catalyst recycling experiments for the hydrosilylation of alkynes catalyzed by heterogeneous catalysts **TRGO-X-Rh**.^{a,b}

entry	alkyne/ silane	Catalyst	Run	t (h)	conv (%)	Selectivity (%)				
										
1	<i>n</i> -HexC≡CH	TRGO-O-Rh	Run 1	0.5	98	99	-	-		
2	/HSiMePh ₂		Run 2	1.5	43	99	-	-		
3	<i>n</i> -HexC≡CH /HSiMe ₂ Ph	TRGO-3-Rh	Run1	0.8	99	93	6	1		
4			Run 2	4	97	92	7	1		
5			Run 3	18	90	90	8	2		
6			Load 2 ^c	1.3	99	96	4	-		
7			Load 3 ^c	2	99	97	3	-		
8			Load 4 ^c	2.8	95	95	5	-		
9			<i>n</i> -HexC≡CH /HSiEt ₃	TRGO-4-Rh	Run 1	1.4	99	82	12	6
10					Run 2	1.4	99	83	11	6
11	Run 3	1.4			98	85	10	5		
12	Run 4	1.4			99	85	11	4		
13	Run 5 ^d	1.4			98	85	10	5		
14	Load 2 ^c	1.4			0	-	-	-		
15	<i>n</i> -HexC≡CH /HSiMe ₂ Ph	TRGO-4-Rh	Run 1	1	95	93	4	3		
16			Run 2	1	97	96	3	1		
17			Run 3	1	94	95	4	1		
18			Run 4	1	96	93	4	3		
19			Run 5 ^d	1	94	94	4	2		
20	<i>n</i> -HexC≡CH /HSiEt ₃	TRGO-4-Rh	Run 1	1.6	98	53	27	20		
21			Run 2	1.6	97	51	29	20		
22			Run 3	1.6	96	54	27	19		
23			Run 4 ^d	1.6	95	53	27	20		
24	Ph-C≡C-Me	TRGO-4-Rh	Run 1	1	98	50	50			
25			Run 2	1	99	52	48			
26			Run 3	1	96	50	50			

a) Conversions and selectivities (%) were calculated by ¹H NMR using anisole as internal standard. b) Experiments were carried out in CDCl₃ (0.5 mL) using a silane/alkyne /catalyst ratio of 100/100/1 with 1 mol% of Rh calculated according to the ICP measurements. c) Consecutive loads of reactants over the resulting solution after removing the heterogeneous catalyst. d) Recycling experiment carried out on air.

Structural properties of recycled catalysts. The recycled **TRGO-4-Rh** catalyst, hereafter named **Recycled a**, recovered after three additional catalytic cycles of hydrosilylation of oct-1-yne with HSiEt₃ (Table 2 entry 23), was analyzed by means of XPS (Table S1, Supporting Information). The analysis confirms the ratio nitrogen/rhodium is close to 3/1 what suggests

that the triazole fragment is maintained after the catalysis. The XPS N1s spectrum exhibits the expected triazole profile (Figure 8a, brown-dashed curve) but slightly shifted at higher binding energies with respect of that of **TRGO-4-Rh** (above 401.5 eV). The widening of the signal might be indicative of some structural changes of the supported catalysts during the catalytic cycles. In this regard, although the C/O atomic ratio is maintained after the catalytic cycles, the carbonaceous structure becomes more disordered as the sp^3 hybridization of the carbonaceous structure increases from 14.5 % to 16.2 %, and the C-X band decreases from 10.1 % in **TRGO-4-Rh** to 8.9 % (Table S1, Supporting Information, **Recycled a**). Moreover, in the XPS O1s spectrum of **Recycled a**, a reduction of the intensity of O-Si signal at higher binding energies is observed (Figure 8b, brown-dashed curve) with respect to that of **TRGO-4-Rh** (Figure 8b, green curve). Additionally, the silicon content decreases after catalysis (from 5.8 % in **TRGO-4-Rh** to 2.5 % in **Recycled a**). Both results point to the elimination of part of the TMS protective groups along the catalytic reaction probably due to the partial lability of these groups. On the other hand, the Rh3d XPS spectra of **Recycled a** (Figure 8c, brown-dashed curve) exhibits the typical bimodal shape but with two maxima in the 3d5/2 peak. Together with the ~308.7 eV, coincident with that of **TRGO-4-Rh** catalyst, another prominent maximum at higher binding energies (~310.0 eV) is observed what might be associated to partial oxidation of the metal center during the catalysis, likely during the last catalytic cycle performed under air, or to the stabilization of rhodium(III) catalytic intermediate species due to a surface effect of triazolylidene functional groups on the nanocarbon walls.

The recycled **TRGO-4-Rh** catalyst recovered after four additional catalytic cycles of the hydrosilylation of oct-1-yne with HSiMePh₂ (Table 2 entry 13), hereafter named **Recycled b**, was also analyzed by means of XPS (Table S1, Supporting Information). In contrast with the silicon content decrease observed for the **Recycled a** sample, a notable increase until 6.9

% was measured for the **Recycled b** material (Table S1, See Supporting Information) but with a drastic decrease of the C-O-Si bonding at higher binding energies in the XPS O1s spectra (Figure 8b, dark green-dotted curve). Thus, it seems that the hydroxyl groups in the material have been deprotected but there is another source of Si apart from that of the original TMS protective group. Furthermore, the amount of sp^2 hybridized carbon atoms in **Recycled b** increases substantially until 83.6 % from the initial 69.3 % found in **TRGO-4-Rh** together with a decrease of sp^3 hybridized carbon atoms (from 14.5 % in **TRGO-4-Rh** to 7.7 % in **Recycled b**). We envisaged that the π - π stacking of the aromatic vinyl-silane products on the graphene sheets could modify the XPS in such a way. The significant carbon and silicon increase observed in the XPS analysis leads to an important decrease of the nitrogen content (from 2.2 % in **TRGO-4-Rh** to 0.9 % in **Recycled b**, Table S1, Supporting Information), although the rhodium content remains constant. Remarkably, the high resolution XPS Rh 3d spectra of **Recycled b** (Figure 8c, dark green-dotted curve) exhibit a shape in the 3d_{5/2} region similar to that for **Recycled a** (Figure 8c, brown-dashed curve) with one maximum at 308.7 eV as in the parent catalysts, and a much less intense shoulder at 310.0 eV than that of **Recycled a**.

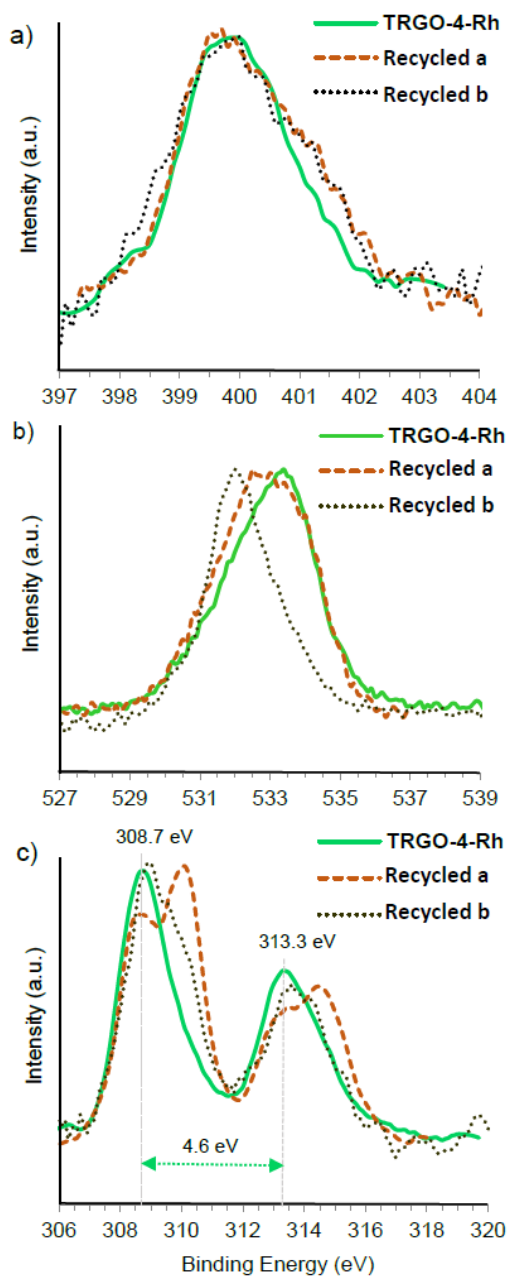


Figure 8. a) XPS N1s spectra, b) XPS O1s spectra and c) XPS Rh 3d spectra, of **TRGO-4-Rh**, **Recycled a** = recycled **TRGO-4-Rh** after hydrosilylation of oct-1-yne with HSiEt₃, and **Recycled b** = recycled **TRGO-4-Rh** after hydrosilylation of oct-1-yne with HSiMePh₂.

In both cases, according to the analysis of the HRTEM images (Figure S26, Supporting Information) and EDX mapping (see Supporting Information), the homogeneous dispersion of the rhodium complexes all over the basal planes of the graphene sheets is mostly maintained after the catalytic runs what evidences the stability of the supported complex during the recycling experiments.

CONCLUSIONS

New alkyne hydrosilylation graphene-NHC-rhodium hybrid catalysts have been synthesized and characterized using a bottom-up approach from thermally reduced graphene oxides (TRGO). First, the carbon materials have been functionalized with triazolium salts covalently attached through C-N bonds to the wall making use of the epoxy functionalities on the solid surface. Then, deprotonation of the acid groups in the materials by $[\text{Rh}(\mu\text{-OMe})(\text{cod})]_2$ results in the formation of rhodium hybrid catalysts. The EXAFS spectra of the resulting molecular anchored materials have allowed us to ascertain the rhodium coordination sphere in the different hybrid materials. It has been found that the deprotonation of the hydroxyl groups on the graphitic support competes with that of the triazolium groups. In this way, the EXAFS analysis has determined that Rh(cod) moieties in the hybrid **TRGO-3-Rh** catalyst are bound to alkoxo ligands from deprotonated hydroxyl groups in the TRGO surface with non-deprotonated triazolium pendant groups. The interference exerted by the hydroxyl groups on the wall of the graphene oxide in the synthesis of a triazolylidene rhodium complex anchored to the carbon nanomaterial is overcome by protection of all -OH groups in the triazolium functionalized material itself with trimethylsilyl group. Thus, the EXAFS spectrum of the silyl-protected **TRGO-4-Rh** material evidenced the presence of rhodium(I)-triazolylidene supported complexes resulting from the selective deprotonation of the triazolium groups by the dinuclear rhodium-methoxo complex.

The graphene-oxide-supported rhodium-triazolylidene, **TRGO-4-Rh**, and rhodium-alkoxo, **TRGO-3-Rh**, hybrid materials, together with the related molecular rhodium-triazolylidene, $[\text{RhI}(\text{cod})(\text{Triaz})]$, compound are efficient catalyst precursors for the hydrosilylation of alkynes. Interestingly, the hybrid rhodium(I) complexes catalyze the hydrosilylation of a range of alkynes, both terminal and internal, with diverse silanes exhibiting high activity and good selectivity to the $\beta(\text{Z})$ vinylsilane, without isomerization

to the more thermodynamically stable $\beta(E)$ vinylsilane isomer, both in acetone and chloroform. Unlike **TRGO-4-Rh**, **[RhI(cod)(Triaz)]** and **TRGO-3-Rh** are active in acetone at room temperature although the later with poor selectivity. Nevertheless, both types of catalysts present very similar reaction profiles that suggest a similar operating mechanism. Moreover, the **TRGO-3-Rh** hybrid catalyst has labile coordination linkages to the nanocarbon materials, and in consequence these materials lost their activity along successive catalytic cycles. In contrast, the heterogeneous catalyst **TRGO-4-Rh** maintains the activity through successive catalytic runs what probes the strength of the C-N covalent bond of the triazolylidene linker to the graphitic wall. Therefore, the supported catalyst can be reused in consecutive cycles without any loss of activity, using different hydrosilanes and alkynes, and even under an air atmosphere.

EXPERIMENTAL

General Considerations. All reactions were carried out under strict exclusion of air using standard Schlenk techniques. Solvents were distilled immediately prior to use from the appropriate drying agents or obtained from a Solvent Purification System (Innovative Technologies). 1,4-Diphenyl-3-methyl-1,2,3-triazolium iodide⁵⁴ and the rhodium starting material $[\text{Rh}(\mu\text{-OMe})(\text{cod})]_2$,⁵⁵ were prepared according to the literature methods. All other reagents were commercially available and used as received.

Specific Equipment. Thermogravimetric analyses (TGA) were performed on a TA SDT 2960 analyzer. The procedure was as follows: 3 mg of sample were heated in the thermobalance to 1000 °C at 10 °C min⁻¹ using a nitrogen:air flow (1:1) of 200 mL min⁻¹. High-resolution transmission electron microscopy (HRTEM) images were obtained using a JEOL JEM-2100F transmission electron microscope, equipped with a field-emission-gun (FEG) and operating at 200 kV. Elemental analyses were carried out on a Perkin-Elmer 2400

Series-II CHNS/O micro-analyzer or a LECO-CHNS-932 micro-analyser equipped with a LECO-VTF-900 furnace coupled to the micro-analyser.

X-ray photoemission spectroscopy (XPS) spectra were performed on a SPECS system operating under a pressure of 10^{-7} Pa with a Mg K α X-ray source. The functional groups in the graphene-based materials were quantified by deconvolution of the corresponding high resolution XPS peaks using a peak analysis procedure that employs a combination of Gaussian and Lorentzian functions and a Shirley baseline.⁵⁶ The spectra did not require charge neutralization and were subsequently calibrated to the C1s line at 284.5 eV. The binding energy profiles for the C1s spectra were deconvoluted as follows: undamaged structures of Csp²-hybridized carbons (284.5 eV), damaged structures or Csp³-hybridized carbons (285.5 eV), C-OH groups (286.5 eV), O-C-O functional groups (287.7 eV) and C(O)OH groups at 288.7 eV. The O1s spectra were deconvoluted using the components C=O/COO (531.7 eV), C-O (533.5 eV) and C-O-Si (533.6 eV). For the N1s spectra, different components were used depending on the nature of the material analyzed and includes -N=N- (400.0 eV), -N- (401.1 eV) and =N⁺= (402.8 eV). The amount of rhodium in the hybrid catalysts was determined by means of Inductively Coupled Plasma Mass Spectrometry (ICP-MS) in an Agilent 7700x instrument.⁵⁷ FTIR spectra were recorded in a Nicolet 8700 spectrometer (Thermo Scientific) using KBr pellets with a sample concentration of ~0.05 wt.%. The recorded spectra were the result of co-adding 64 interferograms obtained at a resolution of 4 cm⁻¹.

X-ray absorption spectroscopy (XAS) measurements at the Rh K edge were recorded at room temperature on the CLAEISS beamline⁵⁸ at the ALBA synchrotron (Cerdanyola del Vallès, Spain). The storage ring was operating at 3 GeV with a current of 120 mA. The EXAFS spectra were measured with a Si (111) double crystal monochromator and harmonic rejection was carried out with a Rh glass strip in the vertical collimator. Estimated energy

resolution, $\Delta E/E$, at the Rh K edge was better than 10^{-4} . The XAS spectra were measured in the transmission mode using pellets diluted with cellulose, if necessary, in order to optimize the absorption jump. The XAS spectra were normalized to unity edge jump and the k weighted EXAFS signals, $k^2\chi(k)$, were obtained using the Athena software from the Demeter package.⁵⁹ The FT curves of the $k^2\chi(k)$ signals were obtained for the $2.9 \leq k \leq 15$ \AA^{-1} range, using a sinus window. The EXAFS structural analysis was performed using theoretical phases and amplitudes calculated by the FEFF-6 code⁶⁰ and fits to the experimental data were carried out in R-space (between 1.1 and 3.0 \AA) with the Artemis program of the Demeter package.⁵⁹

NMR spectra were recorded on a Bruker Advance 300 on a Bruker AV-300 spectrometer (300.13 MHz) in D_2O or acetone- d_6 . Chemical shifts are reported in ppm relative to tetramethylsilane and referenced to partially deuterated solvent resonances. Coupling constants (J) are given in Hertz. Electrospray mass spectra (ESI-MS) were recorded on a Bruker Esquire 3000+ spectrometer using sodium formate as reference. Single crystals of **[RhI(cod)(Triaz)]** for X-ray diffraction studies were grown by slow diffusion of pentane into a concentrated solution of the compound in dichloromethane. X-ray diffraction data were collected at 100(2) K on a Bruker APEX DUO CCD diffractometer with graphite-monochromated Mo-K α radiation ($\lambda = 0.71073$ \AA) using ω rotations. Intensities were integrated and corrected for absorption effects with SAINT-PLUS⁶¹ and SADABS⁶² programs, both included in APEX2 package. The structures were solved by the Patterson method with SHELXS-97⁶³ and refined by full matrix least-squares on F^2 with SHELXL-2014,⁶⁴ under WinGX.⁶⁵

Synthesis of 1,4-diphenyl-1,2,3-triazole.⁵⁴ Phenylazide (490 mg, 4.11 mmol), $CuSO_4 \cdot 5H_2O$ (10.0 mg, 0.041 mmol) and sodium ascorbate (83.1 mg, 0.411 mmol) were dissolved in a deoxygenated t -BuOH/ H_2O mixture (1:1, 2 mL). Then, phenylacetylene (0.9

mL, 8.30 mmol) was added and the resulting mixture vigorously stirred for 16 h at room temperature. The organic layer was washed with water and brine. Removal of the solvent under vacuum afforded the compound as a yellow solid. Yield: 89 %. ^1H NMR (300 MHz, 298K , CDCl_3): δ 7.30 (m, 1H), 7.39 (m, 3H), 7.48 (t, $J = 7.6$, 2H), 7.73 (d, $J = 8.2$, 2H), 7.85 (d, $J = 7.9$, 2H), 8.12 (s, 1H, H_{trz}).

Synthesis of 1,4-diphenyl-3-methyl-1,2,3-triazolium iodide.⁵⁴ 1,4-diphenyl-1,2,3-triazole (370 mg, 1.66 mmol) was dissolved in CH_3CN (30 mL) in a teflon-sealed glass schlenk tube. Then, CH_3I (0.11 mL, 1.83 mmol) was added and the mixture stirred at 372 K overnight. After cooling to room temperature, the yellow precipitated was decanted, washed with CH_3CN (3 x 10 mL) and dried under vacuum. Yield: 71 %. ^1H NMR: (300 MHz, 298K, CDCl_3) δ : 9.74 (s, 1H, H_{trz}), 8.16-8.14 (m, 2H, H_o , NPh), 8.96-8.94 (m, 2H, H_o , Ph), 7.59-7.56 (m, 3H, H_m and H_p , NPh), 7.51-7.48 (m, 3H, H_m and H_p , Ph), 4.44 (s, 3H, NCH_3).

Synthesis of $[\text{RhI}(\text{cod})(\text{Triaz})]$. 1,4-diphenyl-3-methyl-1,2,3-triazolium iodide (100 mg, 0.27 mmol) and $[\text{Rh}(\mu\text{OMe})(\text{cod})]_2$ (65.40 mg, 0.135 mmol) were reacted in THF (10 ml) at room temperature for 5 h. The resulting orange solution was concentrated to ca. 2 mL under reduced pressure. The slow addition of diethyl ether (10 ml) gave a microcrystalline yellow solid which was separated by decantation, washed with diethyl ether (2 x 3 mL) and dried in vacuo. Yield: 89 %. ^1H NMR (300 MHz, 298K, C_6D_6): δ 9.24 (d, 2H, $J_{\text{H-H}} = 8.2$, H_o , NPh), 8.20 (d, 2H, $J_{\text{H-H}} = 7.5$, H_o , Ph), 7.40–7.15 (m, 6H, H_m and H_p , Ph and NPh), 5.77 (m, 2H, CH, cod), 3.40–3.20 (m, 2H, CH, cod), 2.80 (s, 3H, NCH_3), 2.30–1.70 (m, 8H, CH_2 , cod). $^{13}\text{C}\{^1\text{H}\}$ NMR (300 MHz, 298K, C_6D_6) δ : 174.7 (d, $J_{\text{C-Rh}} = 44.5$, $\text{C}_{\text{Rh-trz}}$), 143.8 (C_q , NPh), 140.4 (C_q , Ph), 130.7 (C_o , Ph), 129.0 (d, $J_{\text{C-Rh}} = 5.2$, C_{trz}), 124.1 (C_o , NPh), 128.7 (C_m , Ph and NPh) 128.3 (C_p , Ph and NPh), 94.2 (d, $J_{\text{C-Rh}} = 7.2$, CH, cod), 93.9 (d, $J_{\text{C-Rh}} = 7.3$, CH, cod), 72.8 (d, $J_{\text{C-Rh}} = 14.4$, CH, cod), 70.4 (d, $J_{\text{C-Rh}} = 14.6$, CH, cod), 36.2 (NCH_3), 32.4, (CH_2 , cod), 32.2, (CH_2 , cod), 30.3, (CH_2 , cod), 30.3 (CH_2 , cod). Anal. Calc. for $\text{C}_{23}\text{H}_{25}\text{N}_3\text{RhI}$: C,

48.19; H, 4.00; N, 7.33. Found C, 48.07; H, 3.89; N, 7.53. HRMS (ESI+, CH₃CN, m/z):
Calc. for C₂₃H₂₅N₃Rh: 446.1101. Found for C₂₃H₂₅N₃Rh: 446.1098, [M-I]⁺.

Preparation of partially reduced graphene oxide TRGO-400. Partially reduced graphene oxide **TRGO-400** was prepared by applying a modified Hummers method to commercial graphite as described previously.⁷ The obtained graphite oxide was thermally treated at 300 °C in a pre-heated horizontal furnace, to allow exfoliation and partial reduction, under a nitrogen flow of 50 mL min⁻¹. The obtained graphene material was then thermally treated in a horizontal furnace to 400°C with a residence time at the final temperature of 60 min.

Synthesis of functionalized partially reduced graphene oxides. Synthesis of TRGO-N₃, TRGO-1. Graphene oxide **TRGO-400** (100 mg) was dispersed in a H₂O/CH₃CN mixture (1:1, 10 mL) in an ultrasonic bath for half an hour. Then, NaN₃ (125 mg, 1.92 mmol) was added under argon atmosphere and the black suspension stirred at reflux temperature for one week. After that time, the resulting graphene was washed using the centrifuge with H₂O/CH₃CN (1:1) (4 x 10 ml), H₂O/CH₃CN (1:5) (2 x 10 ml), CH₃CN (2 x 10 ml), and finally with Et₂O (1 x 4 mL) and dried in vacuum.

Synthesis of TRGO-4-phenyl-1,2,3-triazole, TRGO-2. **TRGO-1** (112 mg) was dispersed in a ¹PrOH/H₂O mixture (1:1, 20 mL) in an ultrasonic bath for half an hour. After that, under argon atmosphere, phenylacetylene (0.25 mL, 2.3 mmol), sodium ascorbate (120 mg, 0.61 mmol) and CuSO₄·5H₂O (56 mg, 0.22 mmol) were sequentially added. The suspension was stirred at room temperature for 2 days. Then, the material was washed using the centrifuge with H₂O (4 x 7 mL), acetone (2 x 5 mL), and finally Et₂O (1 x 5mL) and dried in vacuum.

Synthesis of TRGO-3-methyl-4-phenyl-1,2,3-triazolium iodide, TRGO-3. A teflon-sealed glass schlenk tube was charged with a suspension of **TRGO-2** (150 mg) in CH₃CN (25 mL) under argon atmosphere and introduced in an ultrasonic bath for half an hour. Subsequently methyl iodide (1 mL, 3.1 mmol) was added and the suspension was stirred at reflux temperature for 12 h. Then, the graphene was washed using the centrifuge with CH₃CN (4 x 7 mL) and vacuum dried.

Synthesis of TRGO-(SiOMe₃)-3-methyl-4-phenyl-1,2,3-triazolium iodide, TRGO-4. **TRGO-3** (100 mg) was dispersed in freshly distilled anhydrous CHCl₃ (10 mL) in an ultrasonic bath for half an hour and treated with trimethylsilylimidazole (0.15 mL, 0.1 mmol) under argon atmosphere. The suspension was stirred at 60°C for 12 h. The material was washed with CH₂Cl₂ (3 x 6 mL) and dried under vacuum.

Synthesis of supported rhodium catalysts. Synthesis of TRGO-O-Rh. TRGO-400 (40 mg) was dispersed in THF (10 mL) in an ultrasonic bath for half an hour and treated with [Rh(μ-OMe)(cod)]₂ (28.0 mg, 0.058 mmol) at reflux temperature for 24 h under argon atmosphere. After that time, the black solid was washed with THF (5 x 10 mL) and diethyl ether (2 x 5 mL) with the help of ultrasonic bath/centrifuge and dried under vacuum.

Synthesis of TRGO-3-Rh and TRGO-4-Rh. Suspensions of graphene materials functionalized with 3-methyl-4-phenyl-1,2,3-triazolium iodide, **TRGO-3** or **TRGO-4** (100 mg), were dispersed in anhydrous THF (10 mL) in an ultrasonic bath for half an hour and treated, under argon atmosphere, with [Rh(μ-OMe)(cod)]₂ (54.0 mg, 0.105 mmol). The suspension was stirred at 80 °C for 24 h. The solids obtained were washed with THF (5 x 10 mL) and diethyl ether (2 x 5 mL) with the help of ultrasonic bath/centrifuge and dried under vacuum.

Crystal data and structure refinement for [RhI(cod)(Triaz)]. C₂₃H₂₅IN₃Rh·CHCl₃

692.64, 100(2) K, 0.71073 Å, monoclinic, $P2_1/c$, $a = 15.6121(12)$ Å, $b = 8.4405(6)$ Å, $c = 20.6177(15)$ Å, $\beta = 109.5300(10)^\circ$, $V = 2560.6(3)$ Å³, $Z = 4$, $D_{\text{calc}} = 1.797$ g/cm³, $\mu = 2.203$ mm⁻¹, $F(000) = 1360$, yellow prism, 0.260 x 0.140 x 0.050 mm³, $\theta_{\text{min}}/\theta_{\text{max}} 1.384/27.102^\circ$, index ranges $-20 \leq h \leq 20$, $-10 \leq k \leq 10$, $-26 \leq l \leq 26$, reflections collected/independent 27718/5638 [R(int) = 0.0343], data/restraints/parameters 5638/0/290, GOF = 1.063, $R_1 = 0.0262$ [$I > 2\sigma$ (I)], $wR_2 = 0.0596$ (all data), largest diff. peak/hole 0.772/-0.786 e⁻Å⁻³. CCDC deposit number: 1937428

General procedure for catalytic alkyne hydrosilylation reactions. Hydrosilylation catalytic tests were carried out in NMR tubes, under an argon atmosphere, in CDCl₃ or acetone-*d*₆. In a typical procedure, a NMR tube was charged under argon with the catalyst (1x10⁻³ mmol, 1 mol%), deuterated solvent (0.5 mL), the corresponding alkyne (0.1 mmol), hydrosilane (0.1 mmol) and anisole (0.01 mmol) as the internal standard. The solution was kept at room temperature or in a thermostated bath at 60 °C and monitored by ¹H NMR spectroscopy. The weight of the supported catalysts used in each experiment was calculated according to ICP measurements, assuming that all the rhodium in the hybrid materials corresponds to active catalyst sites.

The vinylsilane reaction products derived from 1-alkynes were unambiguously characterized on the basis of the coupling patterns and constants of vinylic protons in the ¹H NMR spectra and subsequent comparison to literature values.⁶⁶ Values for J ranged from 17 to 19 Hz for β -(*E*), 13 to 16 Hz for β -(*Z*), and 1 to 3 Hz for α -vinylsilanes. The vinylsilane reaction products derived from internal alkynes were identified by comparison of NMR data with those previously reported in the literature.⁶⁷

The recycling of the heterogeneous catalyst was carried out by evaporating the deuterated solvent under vacuum. The residue was washed with hexane (3 x 1mL) using the centrifuge to remove the organic products and the residue dried in vacuo. Then, another load of

reactants and deuterated solvent were added in order to perform a new catalytic cycle under the same experimental conditions.

ASSOCIATED CONTENT

Supporting information

The material: Intermolecular contacts in the rhodium molecular complex, additional XPS, TG, Raman, HRTEM, STEM and EDX characterization of TRGO-based materials and detailed XAS analysis of rhodium complexes is available free of charge via the Internet at <http://pubs.acs.org>.

AUTHOR INFORMATION

Corresponding Author

M. Victoria Jiménez: vjimenez@unizar.es, tlf: +34 876553794

Patricia Álvarez: par@incar.csic.es, tlf: +34 985118990,

ORCID

M. Victoria Jiménez: 0000-0002-0545-9107

Beatriz Sánchez-Page: 0000-0002-2449-7459

Jesús J. Pérez-Torrente: 0000-0002-3327-0918

Vincenzo Passarelli: 0000-0002-1735-6439

Javier Blasco: 0000-0002-9706-3272

Gloria Subias: 0000-0002-9029-1977

Marcos Granda: 0000-0001-7479-0445

Patricia Álvarez: 0000-0001-9676-0546

Author Contributions

The manuscript was written through contributions of all authors. All authors have given approval to the final version of the manuscript.

Notes

The authors declare no competing financial interest.

ACKNOWLEDGEMENTS

The authors express their appreciation for the financial support from MICINN/FEDER projects CTQ2016-75884-P and RTI2018-098537-B-C22, and the Regional Governments of Aragón/FEDER 2014-2020 “*Building Europe from Aragón*” (groups E42_17R and E12_17R) and Principado de Asturias (FEDER: IDI/2018/000121) are gratefully acknowledged. The authors also acknowledge ALBA synchrotron for granting beamtime and the collaboration of the CLAESS beamline staff.

REFERENCES

- (1) Hu, M.; Yao, Z.; Wang, X. Graphene-Based Nanomaterials for Catalysis. *Ind. Eng. Chem. Res.* **2017**, *56*, 3477–3502.
- (2) Fan, X.; Zhang, G.; Zhang, F. Multiple Roles of Graphene in Heterogeneous Catalysis. *Chem. Soc. Rev.* **2015**, *44*, 3023–3035.
- (3) Axet, M. R.; Dechy-Cabaret, O.; Durand, J.; Gouygou, M.; Serp, P. Coordination Chemistry on Carbon Surfaces. *Coord. Chem. Rev.* **2016**, *308*, 236–345.
- (4) Bai, L.; Duan, Z.; Wen, X.; Si, R.; Guan, J. *Appl. Catal., B: Environ.* **2019**, *257*, 117930–117937.
- (5) Fei, H.; Dong, J.; Chen, C.; Hu, T.; Duan, X.; Shakir, I.; Huang, Y.; Duan, X. *Chem. Soc. Rev.*, **2019**, *48*, 5207–5241.
- (6) Park, S.; Ruoff, R. S. Chemical Methods for the Production of Graphenes. *Nat. Nanotechnol* **2009**, *4*, 217–224 and references therein.

(7) Botas, C.; Álvarez, P.; Blanco, C.; Santamaría, R.; Granda, M.; Ares, P.; Rodríguez-Reinoso, F.; Menéndez, R. The Effect of the Parent Graphite on the Structure of Graphene Oxide. *Carbon* **2012**, *50*, 275–282.

(8) Hassanpour, A.; Rodríguez-San, D.; Fierro, J. L. G. M.; Horrocks, B. R.; Mas-Ballesté, R.; Zamora, F. Supramolecular Attachment of Metalloporphyrins to Graphene Oxide and its Pyridine-Containing Derivative. *Chem. Eur. J.* **2013**, *19*, 1046–10467.

(9) Avinash, M. B.; Subrahmanyam, K. S.; Sundarayya, Y.; Govindaraju, T. Fundamental Properties of Oligo Double-Stranded DNA/Single-Walled Carbon Nanotube Nanobiohybrids. *Nanoscale* **2010**, *2*, 1762–1766.

(10) Verma, S.; Aila, M.; Kaul, S.; Jain, S. L. Immobilized Oxo-Vanadium Schiff Base on Graphene Oxide as an Efficient and Recyclable Catalyst for the Epoxidation of Fatty Acids and Esters *RSC Adv.* **2014**, *4*, 30598–30604.

(11) Bai C.; Zhao, Q.; Li, Y.; Zhang, G.; Zhang, F.; Fan, X.; Palladium Complex Immobilized on Graphene Oxide as an Efficient and Recyclable Catalyst for Suzuki Coupling Reaction *Catal. Lett.* **2014**, *144*, 1617–1623.

(12) Shang, N.; Gao, S.; Feng, C.; Zhang, H.; Wang, C.; Wang, Z. Graphene Oxide Supported N-Heterocyclic Carbene-Palladium as a Novel Catalyst for the Suzuki–Miyaura Reaction. *RSC Adv.* **2013**, *3*, 21863–21868.

(13) Krabbenborg, R. S. S.; Naber, W. J. M.; Velders, A. H.; Reinhoudt, D. N.; van der Wiel, W. G. The Formation of Large-Area Conducting Graphene-Like Platelets. *Chem. Eur. J.* **2009**, *15*, 8235–8240.

(14) Chen, D.; Feng, H.; Li, J. Graphene Oxide: Preparation, Functionalization, and Electrochemical Applications. *Chem. Rev.* **2012**, *112*, 6027–6053.

- (15) Figueiredo, J. L.; Pereira, M. E. R.; Freitas, M. M. A.; Mórfaõ. J. J. Modification of the Surface Chemistry of Activated Carbons. *Carbon* **1999**, *37*, 1379–1389.
- (16) Cheng, C.; Brookhart, M. Efficient Reduction of Esters to Aldehydes through Iridium Catalyzed Hydrosilylation. *Angew. Chem. Int. Ed.* **2012**, *51*, 9422–9424.
- (17) Ananikov, V. P.; Beletskaya, I. P. Alkyne and Alkene Insertion into Metal-heteroatom and Metal-hydrogen bonds – the Key Stages of Hydrofunctionalization Process. In *Hydrofunctionalization, Top. Organomet. Chem.* **43**. Ananikov, V. P.; Tanaka, M. Eds.; Springer-Verlag, Berlin-Heidelberg, 2012, Chapter 1, pp 1–20.
- (18) Marcienic, B.; Maciejewski, H.; Pietraszuk, C.; Pauluć, P. Hydrosilylation. A Comprehensive Review on Recent Advances. In *Advances in Silicon Science*. Marcienic, B. Ed. Springer Science, 2009.
- (19) Pérez-Torrente, J. J.; Nguyen, D. H.; Jiménez, M. V.; Modrego, F. J.; Puerta-Oteo, R.; Gómez-Bautista, D.; Iglesias, M.; Oro, L. A. Hydrosilylation of Terminal Alkynes Catalyzed by a ONO-Pincer Iridium(III) Hydride Compound: Mechanistic Insights into the Hydrosilylation and Dehydrogenative Silylation Catalysis. *Organometallics* **2016**, *35*, 2410–2422.
- (20) Jiménez, M. V.; Pérez-Torrente, J. J.; Bartolomé, M. I.; Gierz, V.; Lahoz, F. J.; Oro, L. A. Rhodium(I) Complexes with Hemilabile N-Heterocyclic Carbenes: Efficient Alkyne Hydrosilylation Catalysts. *Organometallics* **2008**, *27*, 224 – 234.
- (21) Wang, W.; Lifeng Cui, L.; Peng Sun, P.; Shi, L.; Yue, C.; Li, F. Reusable N-Heterocyclic Carbene Complex Catalysts and Beyond: A Perspective on Recycling Strategies. *Chem. Rev.* **2018**, *118*, 9843–9929.

(22) Lázaro, G.; Fernández-Alvarez, F. J.; Iglesias, M.; Horna, C.; Vispe, E.; Sancho, R.; Lahoz, F. J.; Iglesias, M.; Perez-Torrente, J. J.; Oro, L. A. Heterogeneous Catalysts Based on Supported Rh-NHC Complexes: Synthesis of High Molecular Weight Poly(silylether)s by Catalytic Hydrosilylation. *Catal. Sci. Technol.* **2014**, *4*, 62–70.

(23) Binding, S. C.; Pernik, I.; Gonçalves, V. R.; Wong, C. M.; Webster, R. F.; Cheong, S.; Tilley, R. D.; Garcia-Bennett, A. E.; Gooding, J. J.; Messerle, B. A. Simultaneous Functionalization of Carbon Surfaces with Rhodium and Iridium Organometallic Complexes: Hybrid Bimetallic Catalysts for Hydroamination. *Organometallics* **2019**, *38*, 4, 780-787.

(24) Wong, C. M.; Walker, D. B.; Soeriyadi, A. H.; Gooding, J. J.; Messerle, B. A. A Versatile Method for the Preparation of Carbon–Rhodium Hybrid Catalysts on Graphene and Carbon Black. *Chem. Sci.* **2016**, *7*, 1996–2004.

(25) Ruiz-Botella, S.; Peris, E. Immobilization of Pyrene-Adorned N-Heterocyclic Carbene Complexes of Rhodium(I) on Reduced Graphene Oxide and Study of their Catalytic Activity. *ChemCatChem* **2018**, *10*, 1874–1881.

(26) Blanco, M.; Álvarez, P.; Blanco, C.; Jiménez, M. V.; Pérez-Torrente, J. J.; Oro, L. A.; Blasco, J.; Cuartero, V.; Menéndez, R. Enhancing the Hydrogen Transfer Catalytic Activity of Hybrid Carbon Nanotube-Based NHC-Iridium Catalysts by Increasing the Oxidation Degree of the Nanosupport. *Catal. Sci. Technol.* **2016**, *6*, 5504–5514.

(27) Blanco, M.; Álvarez, P.; Blanco, C.; Jiménez, M. V.; Blasco, J.; Pérez-Torrente, J. J.; Oro, L. A.; Menéndez, R. Enhanced Hydrogen-Transfer Catalytic Activity of Iridium N-Heterocyclic Carbenes by Covalent Attachment on Carbon Nanotubes. *ACS Catal.* **2013**, *3*, 1307–1317.

(28) Nieto, J.; Jiménez, M. V.; Álvarez, P.; Pérez-Mas, A. M.; González, Z.; Pereira, R.; Sánchez-Page, B.; Pérez-Torrente, J. J.; Blasco, J.; Subías, G.; Blanco, M.; Menéndez, R. Enhanced Chemical and Electrochemical Water Oxidation Catalytic Activity by Hybrid Carbon Nanotube-Based Iridium Catalysts Having Sulfonate-Functionalized NHC ligands. *ACS Appl. Energy Mater.* **2019**, *2*, 3283–3296.

(29) EXAFS has been used to determine the local structure in a wide set of compounds including catalysts. See for example: Uzun, A.; Ortalan, V.; Browning, N. D.; Gates, B. C. A Site-isolated Mononuclear Iridium Complex Catalyst Supported on MgO: Characterization by Spectroscopy and Aberration-corrected Scanning Transmission Electron Microscopy. *J. Catal.* **2010**, *269*, 318–328.

(30) Mei, K.; Rubio, N.; Costa P. M.; Kafa H.; Abbate V.; Festy, F.; Bansal, S. S.; Hidera R. C.; Al-Jamal, T. K. Synthesis of Double-clickable Functionalised Graphene Oxide Biological Applications. *Chem. Commun.* **2015**, *51*, 14981–14984.

(31) Lieber, E.; Rao, C. N. R.; Chao, T. S.; Hoffman, C. W. W. Infrared Spectra of Organic Azides. *Anal. Chem.* **1957**, *29*, 916–918.

(32) Halbig, C. E.; Rietsch, P.; Eigler, S. Towards the Synthesis of Graphene Azide from Graphene Oxide. *Molecules* **2015**, *20*, 21050–21057.

(33) Zorn, G.; Liu, L-H.; Árnadóttir, L.; Wang, H.; Gamble, L. J.; Castner, D. G.; Yan, M. X-Ray Photoelectron Spectroscopy Investigation of the Nitrogen Species in Photoactive Perfluorophenylazide-Modified Surfaces. *J. Phys. Chem. C* **2014**, *118*, 376–383.

(34) Fortgang, P.; Tite, T.; Barnier, V.; Zehani, N.; Maddi, C.; Lagarde, F.; Loir, A.; Jaffrezic-Renault N.; Donnet, C.; Garrelie, F.; Chaix. C. Robust Electrografting on Self-Organized 3D Graphene Electrodes. *ACS Appl. Mater. Interfaces* **2016**, *8*, 1424–1433.

(35) For general reviews about triazolylidene complexes see for example: Guisado-Barrios, G.; Soleilhavoup, M.; Bertrand, G. 1H-1,2,3-Triazol-5-ylidenes: Readily Available Mesoionic Carbenes. *Acc. Chem. Res.* **2018**, *51*, 3236–3244.

(36) Silica-supported Rhodium Complexes. Relation between Catalyst Structure and Activity. *J. Molecular Catal.*, **1981**, *11*, 323–330.

(37) NIST X-ray Photoelectron Spectroscopy Database. 2012. <https://srdata.nist.gov/xps/>

(38) Fritsch, A.; Légaré, P. XPS Study of Small Iridium Clusters; Comparison with the Ir₄(CO)₁₂ Molecule. *Surf. Sci.* **1984**, *145*, L517– L523.

(39) Zahmakiran, M. Iridium Nanoparticles Stabilized by Metal Organic Frameworks (IrNPs@ZIF-8): Synthesis, Structural Properties and Catalytic Performance. *Dalton Trans.* **2012**, *41*, 12690–12696.

(40) Greene, T. W.; Wuts, P. G. M. Protective Groups In Organic Synthesis, 3rd ed. John Wiley & Sons: New York, 2007.

(41) Baeza, J. A.; Calvo, L.; Gilarranz, M. A.; Rodriguez, J. J. Effect of Size and Oxidation State of Size-controlled Rhodium Nanoparticles on the Aqueous-phase Hydrodechlorination of 4-Chlorophenol *Chem. Eng. J.* **2014**, *240*, 271–280.

(42) See for example: Aucagne, V.; Leigh, D. A. Chemoselective Formation of Successive Triazole Linkages in One Pot: “Click–Click” Chemistry. *Org. Lett.* **2006**, *8*, 4505–4507.

(43) Poulain, A.; Canseco-Gonzalez, D.; Hynes-Roche, R.; Müller-Bunz, H.; Schuster, O.; Stoeckli-Evans, H.; Neels, A.; Albrecht M. Synthesis and Tunability of Abnormal 1,2,3-Triazolylidene Palladium and Rhodium Complexes. *Organometallics* **2011**, *30*, 1021–1029.

(44) Puerta-Oteo, R.; Jiménez, M. V.; Lahoz, F. J.; Modrego, F. J.; Passarelli V.; Pérez-Torrente J. J. Zwitterionic Rhodium and Iridium Complexes Based on a Carboxylate Bridge-Functionalized Bis-N-heterocyclic Carbene Ligand: Synthesis, Structure, Dynamic Behavior, and Reactivity. *Inorg. Chem.* **2018**, *57*, 5526–5543.

(45) See for example: Palacios, L; Miao, X.; Di Giuseppe, A.; Pascal, S.; Cunchillos, C.; Castarlenas, R.; Pérez-Torrente, J. J.; Lahoz, F. J.; Dixneuf, P. H.; Oro, L. A. Synthesis of a Square-Planar Rhodium Alkylidene N-Heterocyclic Carbene Complex and Its Reactivity Toward Alkenes. *Organometallics* **2011**, *30*, 5208–5213.

(46) Enders, D.; Gielen, H. Synthesis of Chiral Triazolinylidene and Imidazolinylidene Transition Metal Complexes and First Application in Asymmetric Catalysis. *J. Organomet. Chem.* **2001**, *617–618*, 70–80.

(47) Donnelly, K. F.; Lalrempuia, R.; Muller-Bunz, H.; Albrecht, M. Regioselective Electrophilic C–H Bond Activation in Triazolylidene Metal Complexes Containing a N-Bound Phenyl Substituent *Organometallics*, **2012**, *31*, 8414–8419.

(48) Azpíroz, R.; Rubio-Pérez, L.; Di Giuseppe, A.; Passarelli, V.; Lahoz, F. J.; Castarlenas, R.; Pérez-Torrente, J. J.; Oro, L. A. Rhodium(I)-N-Heterocyclic Carbene Catalyst for Selective Coupling of N-Vinylpyrazoles with Alkynes via C–H Activation. *ACS Catal.* **2014**, *4*, 4244–4253.

(49) Brookhart, M.; Green, M. L. H.; Parkin, G. Agostic Interactions in Transition Metal Compounds. *Proc. Natl. Acad. Sci. U.S.A.* **2007**, *104*, 6908–6914.

(50) Harrison, J. A.; Nielson, A. J.; Sajjad, M. A.; Saunders, G. C.; Schwerdtfeger, P. Steric and Electronic Manipulation of the Anagostic Interaction in 1-Tetralone Oxime and Imine Complexes of Rhodium(I). *Eur. J. Inorg. Chem.* **2016**, 64–77.

(51) Iglesias, M.; Pérez-Nicolás, M.; Sanz Miguel, P. J.; Polo, V.; Fernández-Alvarez, F. J.; Pérez-Torrente, J. J.; Oro, L. A. A Synthon for a 14-electron Ir(III) Species: Catalyst for Highly Selective β -(Z) Hydrosilylation of Terminal Alkynes. *Chem. Commun.* **2012**, *48*, 9480–9482.

(52) Busetto, L.; Cassani, M. C.; Femoni, C.; Mancinelli, M.; Mazzanti, A.; Mazzoni, R.; Solinas, G. N-Heterocyclic Carbene-Amide Rhodium(I) Complexes: Structures, Dynamics, and Catalysis. *Organometallics* **2011**, *30*, 5258–5272.

(53) Rhodium(I) complexes can promote undesirable polymerization of aryl-substituted alkynes such as phenylacetylene. See, for example: Mori, A.; Takahisa, E.; Yamamura, Y.; Kato, T.; Mudalige, A. P.; Kajiro, H.; Hirabayashi, K.; Nishihara, Y.; Hiyama, T. Stereodivergent Syntheses of (Z)- and (E)-Alkenylsilanes via Hydrosilylation of Terminal Alkynes Catalyzed by Rhodium(I) Iodide Complexes and Application to Silicon-Containing Polymer Syntheses. *Organometallics* **2004**, *23*, 1755–1765.

(54) Poulain, A.; Canseco-Gonzalez, D.; Hynes-Roche, R.; Müller-Bunz, H.; Schuster, O.; Stoeckli-Evans, H.; Neels, A.; Albrecht M. Synthesis and Tunability of Abnormal 1,2,3-Triazolylidene Palladium and Rhodium Complexes. *Organometallics* **2011**, *30*, 1021–1029.

(55) Uson, R.; Oro, L. A.; Cabeza, J. A. Dinuclear Methoxy, Cyclooctadiene, and Barrelene Complexes of Rhodium(I) and Iridium(I). *Inorg. Synth.* **1985**, *23*, 126–130.

(56) Sherwood, P. M. A. In *Practical Surface Analysis in Auger and X-ray Photoelectron Spectroscopy*; Briggs, D.; Seah, M. P. Eds.; Wiley: New York, 1990, 2nd ed. vol. 1, pp. 657.

(57) Elgrabli, D.; Floriani, M.; Abella-Gallar, S.; Meunier, L.; Gamez, C.; Delalain, P.; Rogerieux, F.; Boczkowski, J.; Lacroix, G. Biodistribution and Clearance of Instilled Carbon Nanotubes in Rat Lung. *Part. Fibre. Toxicol.* **2008**, *5*, 20–33.

(58) Simonelli, L.; Marini, C.; Olszewski, W.; Avila, M.; Ramanan, N.; Guilera, G.; Cuartero, V.; Klementiev, K. CLÆSS: The Hard X-ray Absorption Beamline of the ALBA CELLS Synchrotron. *Cogent Physics* **2016**, *3*, 1231987.

(59) Ravel, B.; Newville, M. ATHENA, ARTEMIS, HEPHAESTUS: data analysis for X-ray absorption spectroscopy using IFEFFIT. *J. Synchrotron Radiat.* **2005**, *12*, 537–541.

(60) Rehr, J. J.; Albers, R. C. Theoretical Approaches to X-ray Absorption Fine Structure. *Rev. Mod. Phys.* **2000**, *72*, 621–654.

(61) SAINT+: Area-Detector Integration Software, version 6.01; Bruker AXS: Madison, WI, 2001.

(62) Sheldrick, G. M. SADABS program; University of Göttingen: Göttingen, Germany, 1999.

(63) Sheldrick, G. M. SHELXS 97, Program for the Solution of Crystal Structure; University of Göttingen: Göttingen, Germany, 1997.

(64) Sheldrick, G. M. Crystal structure refinement with SHELXL. *Acta Crystallogr., Sect. C: Struct. Chem.* **2015**, *71*, 3–8.

(65) Farrugia, L. J. WinGX and ORTEP for Windows: an update. *J. Appl. Crystallogr.* **2012**, *45*, 849–854.

(66) (a) Derivatives from *n*-BuC≡CH: Jun, C. H.; Crabtree, R. H. Dehydrogenative Silation, Isomerization and the Control of *syn*- vs. *anti*-addition in the Hydrosilation of Alkynes. *J. Organomet. Chem.* **1993**, *447*, 177–187. (b) Derivates from *n*-HexC≡CH: Nakamura, S.; Uchiyama, M.; Ohwada, T. Chemoselective Silylzincation of Functionalized Terminal Alkynes Using Dianion-Type Zincate (SiBNOL-Zn-ate): Regiocontrolled

Synthesis of Vinylsilanes. *J. Am. Chem. Soc.* **2004**, *126*, 11146–11147. (c) Derivates from $t\text{-BuC}\equiv\text{CH}$: Andavan, G. T. S.; Bauer, E. B.; Letko, C. S.; Hollis, T. K.; Tham, F. S. Synthesis and Characterization of a Free Phenylene bis(N-heterocyclic carbene) and its di-Rh Complex: Catalytic Activity of the di-Rh and CCC-NHC Rh Pincer Complexes in Intermolecular Hydrosilylation of Alkynes. *J. Organomet. Chem.* **2005**, *690*, 5938–5947. (d) Derivatives from $\text{PhC}\equiv\text{CH}$: Katayama, H.; Taniguchi, K.; Kobayashi, M.; Sagawa, T.; Minami, T.; Ozawa, F. J. Ruthenium-Catalyzed Hydrosilylation of Terminal Alkynes: Stereodivergent Synthesis of (*E*)- and (*Z*)-Alkenylsilanes. *J. Organomet. Chem.* **2002**, *645*, 192–200.

(67) (a) Derivatives from $\text{PhC}\equiv\text{CPh}$: Žak, P.; Bolt, M.; Kubicki, M.; Pietraszuk, C. Highly Selective Hydrosilylation of Olefins and Acetylenes by Platinum(0) Complexes Bearing Bulky N-heterocyclic Carbene Ligands. *Dalton Trans.* **2018**, *47*, 1903–1910. (b) Derivates from $\text{PhC}\equiv\text{CMe}$: Gee, J. C.; Fuller, B. A.; Lockett, H.-M.; Sedghi, G.; Robertson, C. M.; Luzyanin, K. V. Visible Light Accelerated Hydrosilylation of Alkynes Using Platinum–[Acyclic Diaminocarbene] Photocatalysts. *Chem. Commun.* **2018**, *54*, 9450–9453.

For Table of Contents (TOC)

